ATTACHMENT 1

NEW YORK UNIVERSITY

College of Engineering

RESEARCH DIVISION

University Heights, New York 53, N. Y.

Department of Meteorology and Oceanography
Geophysical Sciences Laboratory Report No. 63-2

WIND TUNNEL TESTS OF GAS DIFFUSION FROM A LEAK IN THE SHELL OF A NUCLEAR POWER REACTOR AND FROM A NEARBY STACK

James Halitsky
Jack Golden
Paul Halpern
Paul Wu

Prepared for

Environmental Meteorological Research Project
United States Weather Bureau
Washington 25, D. C.

Contract No. Cwb-10321

April 1, 1963

NEW YORK UNIVERSITY
COLLEGE OF ENGINEERING
RESEARCH DIVISION

Department of Meteorology and Oceanography
Geophysical Sciences Laboratory Report No. 63-2

WIND TUNNEL TESTS OF GAS DIFFUSION FROM A LEAK IN THE SHELL OF A NUCLEAR POWER REACTOR AND FROM A NEARBY STACK

By

James Halitsky
Jack Golden
Paul Halpern
Paul Wu

Prepared for
Environmental Meteorological Research Project
United States Weather Bureau
Washington 25, D. C.
Contract No. Cwb - 10321

April 1, 1963

ABSTRACT

Tests were conducted in the NYU $3\frac{1}{2}$ x 7 ft low speed wind tunnel to determine the distribution of gas concentrations resulting from a gas leak in the shell of an industrial nuclear power reactor. The shell was patterned after the EBRII reactor at the NRTS at Idaho Falls. The basic tests were made on the shell alone in an adiabatic atmosphere having a logarithmic velocity profile corresponding to an average profile at NRTS. Additional tests showed the effect of a uniform velocity profile, change of absolute wind velocity, inclusion of auxiliary buildings and heating the shell. The effect of proximity of the stack top to the shell was studied briefly.

TABLE OF CONTENTS

LIST OF FIGURES

LIST OF TABLES

LIST OF SYMBOLS

A = area of the projection of the shell on a plane transverse to the background flow direction

A' = plume cross-section area = $2\pi (x\sigma_q/V)^2$

c = local time-mean concentration

c_{av} = $\dot{Q}/A'V$

D = shell diameter in plan view = 80 ft

$_f$ = subscript denoting full scale

H = shell height = 98 ft

K = experimentally determined distribution function = $cAV/\dot{Q}$

K' = Hay-Pasquill distribution function for a plume from a continuous point source = $\exp\left\{-r^2/2(x\sigma_q/V)^2\right\}$

L = reference length

$_m$ = subscript denoting model

q = general velocity component in isotropic turbulence

$\dot{Q}$ = volume flow rate of gas component of effluent

r = radial coordinate = $\sqrt{y^2+z^2}$

$_s$ = subscript denoting distance in isotropic turbulence

S = distance measured radially outward from shell surface

u,v,w = general velocity components in the x, y, z directions

$\bar{u}$ = local mean velocity in the x direction

u_* = friction velocity = $\sqrt{\text{shear stress/density}}$

U = reference velocity for tunnel airstream or full scale wind

V = general reference velocity

V_e = velocity of effluent at exhaust aperture

x,y,z = general coordinates: downwind, lateral, up, respectively

X,Y,Z = distances in the tunnel along coordinate axes

Z_o = surface roughness parameter

θ = azimuth angle from upwind direction

σ_q = r.m.s. velocity fluctuation in isotropic turbulence

σ_s = r.m.s. distance of concentration distribution

σ_θ = r.m.s. gust angle (radians)

1. INTRODUCTION

Nuclear power reactors are generally enclosed in a gas-tight shell which serves to prevent the uncontrolled release of radioactive gas or air to the atmosphere. In normal operation, the air within the shell becomes irradiated and must be replaced periodically. In order to protect people residing or working in the vicinity of the reactor, the contaminated air is usually discharged through a stack when meteorological conditions are favorable. In the event of a power excursion, the shell will retain the fission products until such time as they may be released safely through the stack. There is the possibility, however, that the shell will be breached during an excursion, resulting in the escape of radioactive gas directly to the atmosphere. In this case personnel must be evacuated from areas likely to become contaminated.

In order to realistically prescribe safe gas or air release rates from the stack, and to delineate danger areas resulting from gas leaks, it is necessary to calculate the field of gas concentration created by a source located arbitrarily at any point on the surface of the reactor shell or at the top of a stack located near the reactor. Unfortunately, the well-known continuous point-source diffusion formulas cannot be used for gas leaks or for stacks that do not rise considerably above the reactor and auxiliary buildings. These formulas were derived under the assumption that the flow field into which the gas is released has straight, parallel mean streamlines and homogeneous turbulence. This assumption is evidently invalid near buildings where the streamlines curve strongly near the upwind face, and almost disintegrate into a confused field of variable, high turbulence near the downwind face.

The experimental approach is the only one that gives any promise of producing reasonably accurate estimates of gas diffusion near buildings at the present time. Two types of experiments are possible: full scale and wind tunnel model tests. In a given configuration, the full scale test will give the most direct and reliable data. However, the cost of a comprehensive test series is considerable, particularly if one wishes to systematically evaluate the effect of changes in source location and wind direction. Practically, the wind tunnel test is the more desirable approach, but its use can be justified only if questions of flow simulation and scaling can be resolved. These are discussed in detail in Ref 1, where it is concluded that diffusion patterns around sharp-edged buildings in an adiabatic atmosphere can be modeled if geometric similarity of the model and dynamic similarity of the free stream are preserved, and the Reynolds Number is not too low. Ref 1 also proposes a method of presenting concentration data in non-dimensional form, thus enabling the scaling up of model results.

Confirmation of the validity of model diffusion testing by direct comparison with full-scale tests has not received much attention. However, in reporting on one such correlation test of gas released in the streets of a model city, Ref 4 states that the concentrations predicated by the wind tunnel tests fall within the range measured in the field under a not-too-steady atmospheric condition, thereby implying that tunnel tests are, at least, a good approximation to field tests.

The principal purpose of the tests described in this report was to determine characteristic diffusion patterns around gas leaks at arbitrary locations on the surface of a typical nuclear reactor shell. The EBRII reactor at the National Reactor Testing Station at Idaho Falls, Idaho was used as a model. Most of the tests were conducted with the reactor alone on the bare floor of the wind tunnel in a wind stream having a logarithmic mean velocity profile scaled down from an average profile measured at NRTS. A few exploratory tests were made to determine the effects of surrounding the reactor with the buildings that exist at NRTS, changing the velocity profile from logarithmic to uniform, increasing and decreasing the wind velocity, and raising the surface temperature of the reactor shell. A few tests were also made to determine ground concentrations resulting from gas released through a stack near the shell.

The tests were sponsored by the Environmental Meteorological Research Project of the U. S. Weather Bureau, in collaboration with the Environmental and Sanitary Engineering Branch, Division of Reactor Development, U. S. A. E. C., Germantown, Md. Personnel of the W. B. Research Station at NRTS cooperated in providing physical dimensions and wind data at the Station.

2. TEST APPARATUS AND PROCEDURE

2.1 Wind Tunnel

The New York University $3\frac{1}{2}$x7 ft wind tunnel, in which these tests were conducted, was designed specifically for the study of air flow phenomena associated with the dispersal of stack gases. The tunnel is of the open return type, the air being drawn from within the laboratory building and exhausted out through the roof. The three main parts of the tunnel are: (1) inlet section, (2) test section and (3) air driving and exhaust section.

The function of the inlet section is to produce an air stream of uniform velocity and temperature at the entrance to the test section. The inlet section contains fans and thermostatically controlled heaters to raise the temperature of the intake air to about 10F above building ambient temperature. The fans prevent thermal stratification. Three fine-mesh screens in an expansion section, followed by a contraction cone, reduce air turbulence to an extremely low value and produce a substantially constant velocity distribution.

The test section is seen in Fig 2. It is basically a horizontal rectangular duct 7 ft wide x $3\frac{1}{2}$ ft high x 40 ft long. A grid of horizontal electric heating wires spaced 10 per inch vertically is stretched across the air stream 1 ft upwind of the test section. Although not used in these tests, the heating grid provides a means for introducing a vertical temperature gradient in the air stream as it moves into the test section. The floor and ceiling of the test section are of sheet steel construction and are temperature-controlled for their entire lengths. The left wall of the test section (looking upwind) has a series of windows beginning 10 ft from the upwind end. The right wall is of plywood construction. Two rails on the ceiling support a survey carriage which positions instrument probes in three dimensions by remote control.

The driving and exhaust section is located downwind of the test section. It contains an electrically driven fan that produces continuously-variable air velocities in the range 0 - 20 fps.

2.2 Model

The model consisted of the reactor shell, the stack and the auxiliary buildings constructed to a linear scale of 1 inch = 8 ft, or 1:96. The basic feature of the topography, its flatness, was reproduced by placing the model on the tunnel floor. The surface roughness, consisting of 20-inch sagebrush covering 20% of the area, was not reproduced. Figs 1 and 2 show an aerial view of the prototype and two views of the model in the tunnel.

The model was built to dimensions taken from a plot plan of the NRTS area, DWG. EBRII-101-1D0-1 Rev 1, dated 5/28/58. Subsequently, an aerial photograph, taken July 28, 1961, was provided, from which the size and location of actual buildings could be determined. Some discrepancies were found in the locations of several of the buildings. Fig 3 shows the model as constructed. Fig 4 shows the actual situation, with the model

building outlines superimposed as dashed lines. Auxiliary buildings were constructed of 1/8 inch cardboard; only the gross features of the buildings were reproduced.

The dimensions of the reactor shell, in terms of full-size feet and fraction of reactor diameter, are shown in Fig 5. Two models of the shell having identical external contours were used during the test. The first of these, unheated, consisted of a cylindrical lower section of brass tubing having a 10 inch O.D. and a hemispherical solid wood dome of 5 inch radius. The entire model shell stood 12.25 inches high. Apertures of 0.063 inch diameter, were provided at 0.75 inch and 7.75 inch above the base of the cylinder (along a vertical line) and at the top of the dome, to serve as gas leakage points. Individual sections of 0.094 inch I.D. copper tubing connected each aperature to an SO_2 source outside the tunnel. Only one line was used at a time, the remaining lines being capped to avoid leakage into the tunnel.

The heated shell was similar to the unheated shell, but its dome was of $\frac{1}{4}$ inch thick brass. Heating elements were mounted within the shell, and thermocouples were placed in the shell to enable monitoring of the shell temperature. The current input to the heating coils was adjustable, and the shell's temperature could be maintained at any value from tunnel ambient temperature (85°F) to 400°F above ambient. The leakage points and connections in this model were identical with those of the unheated model.

The prototype stack is 100 ft high and has an I.D. of 5 ft. These dimensions were approximated by a 12.5 inch length of 5/8 inch O.D. tubing (0.578 inch I.D.). Stack extensions consisted of additional lengths of identical tubing.

2.3 Wind Velocity Profiles

The wind velocity in the empty test section is uniform in each cross-section except in the boundary layers, which are about 4 inches thick at the model location. Therefore, the full scale equivalent vertical velocity profile would consist of a ground boundary layer about 30 ft high, above which the velocity is uniform to a height of about 300 ft. For convenience, this profile will be designated "uniform".

The uniform profile can be modified by inserting horizontal plates in the upwind end of the test section. The desired profile is obtained by adjusting the plate spacing and adding roughness strips to each plate. The profile so produced decays over the length of the test section, but is reasonably stable over the 15 ft length occupied by the model.

In most of the tests in this series, the plates were adjusted to reproduce the profile measured at NRTS in moderate winds and adiabatic conditions. According to data from NRTS, representative full scale wind parameters are $u_* = 25$ cm/sec (0.82ft/sec) and $Z_o = 1.5$ cm (0.0492 ft). When reduced in a velocity scale of 1:3 and a linear scale of 1:96, these parameters become $u_* = 0.273$ ft/sec and $Z_o = 0.000513$ ft. Assuming $k = 0.4$, the equations of the full scale and model profiles become

full scale: $\bar{u}_f = 2.05 \ln(Z_f/.0492)$ (1)

model : $\bar{u}_m = 0.683 \ln(Z_m/0.000513)$, (2)

where $\bar{u}$ = mean velocity, ft/sec, at height Z

Z = elevation, ft, above ground

m and f = model and full scale

For convenience, this profile will be designated "logarithmic". The full scale logarithmic profile is shown in Fig 5, together with the equivalent location of the tunnel ceiling and its boundary layer.

The adjustment of the profile plates was guided by vertical velocity traverses with a hot-wire anemometer probe at the location of the reactor shell in the absence of the model. After the desired profile was achieved, the plate arrangement was not changed for the entire series of logarithmic profile tests. Although the tunnel was shut down overnight, the profile was recovered without difficulty by adjusting the propeller speed to produce the same velocity at a given elevation. This elevation was arbitrarily chosen as 20 inches in the tunnel (160 ft full scale); the corresponding mean velocity was 5.54 ft/sec (16.7 ft/sec full scale). When the model was placed in the tunnel, the traverse rod was re-located 3 ft upwind and 1.67 ft to the side of the reactor, as shown in Fig 2. A vertical velocity traverse was made at the start of each test day. The velocity at the 20-inch elevation was monitored constantly during the tests.

2.4 Gas Tracer Technique

After the flow in the tunnel stabilized, SO_2 was released from the model, and samples of air from the vicinity of the model were withdrawn from the tunnel and analysed. The apparatus used for dispensing the gas and analysing the sample consisted of a metering bench and a Consolidated Titrilog, somewhat modified to suit the particular needs of the tunnel. A complete description of the gas system may be found in Ref 1.

In this test, samples were taken in the air around the model, along the surface of the model, and along the ground. At the model, the tip of the 1/16 inch I.D. probe was placed 0.1 in (0.8 ft full size) from the surface. When measuring ground concentrations, the probe tip was placed 0.5 inch (4 ft full size) above the tunnel floor. The probe was mounted on an out-rigger extending forward of the control carriage in order to minimize flow disturbances that might be introduced by the carriage. The sample aspiration rate was maintained constant at 900 cc/min.

The pure gas release rate from the shell orifices varied from 6.8 to 300 cc/min, according to the location of the sampling probe; the larger rate was used for traverses considerably downwind of the shell, for configurations involving the shell in the complex, and for the heated shell tests. The emission velocities from the 0.063 inch diameter orifices, corresponding to the above flow rates, were 0.2 to 8.1 ft/sec, respectively.

In the stack tests, the gas component of the effluent mixture varied from 100 to 1010 cc/min, while the emission velocity was maintained constant at 4.6 ft/sec.

2.5 Photographic Technique

In order to obtain a visible record of gas and air motions in the vicinity of the reactor, smoke was released at various points near the reactor surface, and single-flash photographs were taken with cameras mounted above and to the side of the reactor. The oil-fog smoke was produced by a special generator located outside the tunnel, and brought through the tunnel wall by means of a rubber tube terminating at a nozzle having an inside diameter of 0.45 inch. The tip of the nozzle was placed within 0.5 inch of the reactor surface, and smoke was released at a speed of about 5 ft/sec while the tunnel velocity was maintained constant at 2 ft/sec. These conditions were optimum for the smoke photographs but were not used in, and do not represent, the gas tracer test conditions. The smoke nozzle was positioned for each photograph so that the smoke was released normal to a solid surface, thus dissipating the momentum of the jet and allowing the smoke to assume the local air velocity quickly.

To provide the necessary lighting, two special strobe tubes were mounted under the tunnel ceiling directly over the model. A Leica IF camera with a 3.5 cm wide-angle lens was used with Plux X film and a shutter speed of f/16. The camera is shown mounted in its ceiling location, but without the strobe lights, in Fig 2.

3. TEST PROGRAM AND RESULTS

3.1 Test Program

The test program consisted of (1) a qualitative study of the field around the reactor shell by visual observation of the travel of smoke released near the shell, and (2) a quantitative study of gas concentrations produced by the release of gas through orifices in the shell and through a nearby stack. The test conditions for the latter study are summarized in Tables 1 and 2.

Locations in the tunnel are referred to a right hand coordinate system originating at the center of the base of the reactor shell on the tunnel floor. The coordinate axes are oriented parallel to the tunnel axes: X = longitudinal, positive downwind; Y = lateral, positive to left looking downwind; Z = vertical, positive up. Linear dimensions are expressed as equivalent full scale feet, or as non-dimensional ratios referred to the reactor shell diameter D = 80 ft. In the case of stack releases only, the non-dimensional ratios are referred to the reactor shell height H = 98 ft.

Unless otherwise noted, the term wind velocity refers to the velocity at the reference elevation of 20 inches in the tunnel, and is designated by U, with appended subscript $_m$ or $_f$ to indicate model or full scale. The wind velocity profiles are designated as either logarithmic or uniform; the profile details are given in Sec 2.3.

The surface temperature differential listed in Table 2 is the nominal excess of shell temperature over the uniform temperature of the tunnel wind stream. The differential is actually the average of four readings, two in the dome surface and two in the cylinder surface, symmetrically disposed on the upwind and downwind centerlines. Due to poor heater location, the dome temperature was considerably higher than the cylinder temperature. The actual temperature distributions during the two heated shell tests are given in Table 3.

3.2 Test Results

The test results consist of photographs showing the general nature of air flow and diffusion in the vicinity of the reactor (Figs 6 and 7), and graphs of concentration coefficient isopleths (Figs 8 to 36). It will be helpful if the results are viewed against a background of a general understanding of cavity and wake flow behind objects. The subject is covered in considerable detail in Ref 1, but some of the material pertinent to flow around spherical domes will be repeated here for the reader's convenience.

3.21 General Nature of Flow Fields Near Objects

The flow field around an object in a wind stream contains several zones having markedly different characteristics:

a) Adjacent to each surface, and completely surrounding the object, there exists a thin boundary layer in which the mean velocity increases asymptotically from zero at the object surface to a slowly-varying value in the outer portion of the boundary layer.

b) Outside of the boundary layer and immediately downwind of the object, there exists an ellipsoidal region called a cavity in which the velocities and pressures are low and the turbulence is very high.

c) Surrounding the cavity and extending a considerable distance downwind from the object, there exists a paraboloidal region called a wake, characterized by ambient pressures and velocities lower than free-stream velocity.

d) Surrounding the wake and the upwind boundary layer, there exists a region called a displacement zone in which the fluid is displaced laterally as it flows around the object and the wake. The flow in the displacement zone is substantially potential, and is characterized by well-defined, curved streamlines, low turbulence, and pressures and velocities related through Bernoulli's Law along a streamline.

e) The object and its boundary layer, cavity, wake and displacement zone are all immersed in the background flow, which, in the case of a building resting on the ground, is the earth's boundary layer.

The sketch on the following page shows how these zones are arranged about the reactor shell. The sketch is approximate, since no velocity measurements were taken other than in the background flow. The zone boundaries were established as follows:

a) between background and displacement flows or between background and wake flows: the surface at which the local velocity deviates more than 5% in magnitude or direction from the velocity of the background flow in the absence of the object,

b) between displacement flow and upwind boundary layer or between displacement and wake flows: the surface at which the velocity deviates more than 5% from the (theoretical) potential flow velocity around the object,

c) between wake and cavity flows: the streamline surface within the wake, separating the circulatory flow within the cavity from the consistently downwind flow in the balance of the wake.

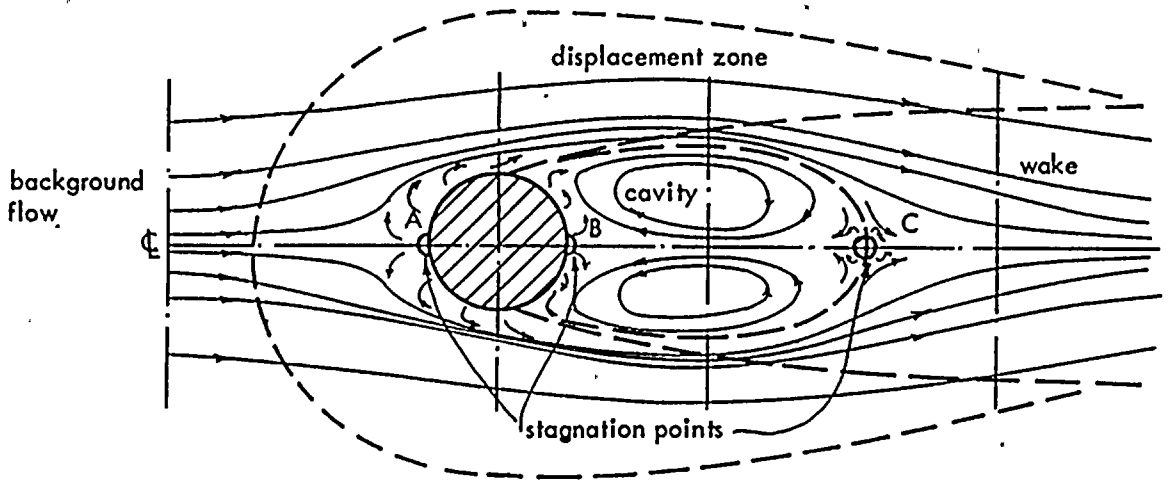

a) Flow in a horizontal plane near the ground

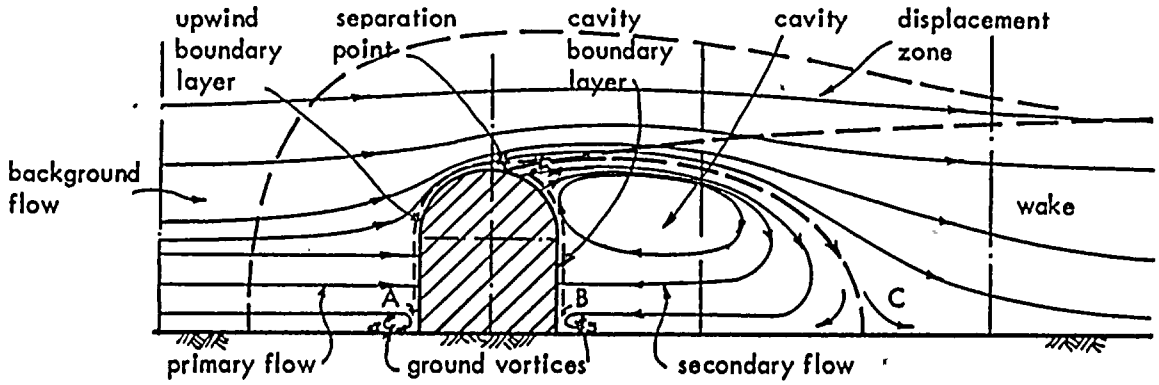

b) Flow in the longitudinal centerplane

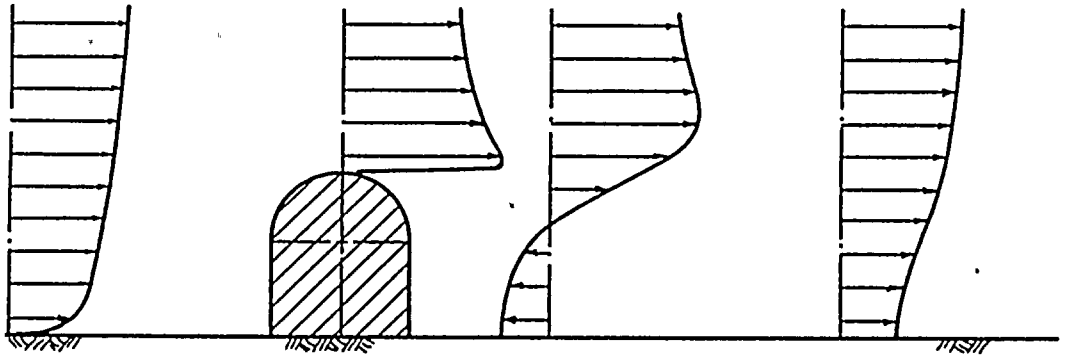

c) Velocity profiles in the longitudinal centerplane

Sketch of Flow Patterns near the Reactor Shell

A very important characteristic of flow around objects is the existence of the cavity. The cavity is generated when the upwind boundary layer separates from the surface of the object, and prevents the potential flow from following the object contours. The dimensions of the cavity, and the velocities and pressures within it, depend principally on the velocity and pressure of the potential flow at the line of separation. On an object with rounded surfaces, the line of separation is near the intersection of the object surface and a transverse plane through its maximum cross-section. Along this line, the potential velocities are a maximum (25-50% higher than the background flow) and the static pressures are a minimum for the entire flow field. The streamlines originating at the line of separation, and forming the upwind portion of the cavity boundary, are only slightly concave toward the axis of the object; therefore, the velocities and pressures along this part of the cavity boundary are fairly constant and equal to the velocities and pressures at the line of separation. The pressure within the cavity is basically the same as at the boundary.

At the downwind end of the cavity, the boundary collapses toward the axis, and the streamlines converge to a common point at the ground, forming a stagnation point (at C in the sketch), where the velocity is zero and the pressure is somewhat higher than the background flow pressure. Thus the pressure gradient along the ground is such as to induce a flow from the stagnation point C toward the object, as well as from the stagnation point downwind. The upwind flow near the axis of the cavity combines with the downwind flow near the cavity boundary to form a toroidal vortex within the cavity. All flow downwind of the cavity is in the same direction, producing the characteristic wake velocity pattern of low velocity near the axis increasing to the background flow velocity radially outward and longitudinally downwind. Velocity profiles at various longitudinal stations are shown in the sketch.

If one is interested only in the flow pattern in the immediate vicinity of the object, one may ignore the downwind part of the cavity and view the object as being exposed simultaneously to a strong primary (downwind) flow and a weak secondary (upwind) flow. These two flows produce stagnation zones of local high pressure and zero velocity at the upwind and downwind portions of the object surface(at A and B in the sketch). The high pressures cause the ground boundary layers of the primary and secondary flows to separate from the ground near the base of the object, and form ground vortices directed down along the base of the object and radially outward along the ground. If the ground boundary layer is thick, the kinetic energy of the primary and secondary flows in the lowest layers will be very small, allowing the radial outward flow caused by the vortices to extend a considerable distance from the base of the object.

Both primary and secondary flows accelerate around the object from stagnation regions A and B to high velocity regions near the lateral periphery of the object, where they combine and leave the surface. The line of separation is the juncture of the surface boundary layers produced by the primary and secondary flows. The position of the separation line is quite sensitive to the relative kinetic energies of the two flows. The distribution of kinetic energy within each flow is different. The primary flow has principally high velocity and low turbulence, and therefore, has a

high proportion of ordered energy. The secondary flow has low velocity and extremely high turbulence; therefore the ordered energy is smaller. This imbalance of ordered but oppositely-directed energy always produces boundary layer separation downwind of the maximum cross-section of a rounded object. When conditions are such that the ordered kinetic energy in one of the two boundary layers is increased, that boundary layer will remain attached to the surface for a greater distance. An increase of turbulence in the background flow will carry ordered energy from the primary flow into the primary boundary layer, thus driving the line of separation downwind, thereby reducing the size of the cavity, increasing the cavity pressure and weakening the toroidal vortex.

3.22 Smoke Photographs

The smoke sequence of Fig 6 shows top and side views of smoke-patterns produced when smoke is released at points successively farther downwind in the longitudinal centerplane but along the solid surface of the ground or shell. The length of the side of each square in top view is equal to the shell diameter D. The proximity of the camera makes the dome seem oversized. In side view, true distances may be scaled along the tunnel centerline through the base of the shell. Top and side views were not photographed simultaneously; the pictures do not correspond exactly due to the turbulent nature of the flow.

In Frame 1 the flow at the ground appears to move as in potential flow around the shell. In Frame 2, however, the clockwise-rotating ground vortex shows up clearly in side view, and the top view shows that the vortex carries gas almost D/2 upwind from the shell surface. In Frame 3 the effect of the ground vortex is even more apparent. The vortex core has bent into a horseshoe around the shell, inducing a downflow along the lower upwind surface; therefore, smoke from the nozzle moves diagonally downwind and down. Frame 4 shows the effect of introducing buildings upwind of the shell without moving the probe. The cavities created by these buildings completely destroy the flow pattern, and draw smoke upwind to the boundaries of the building cavities.

The flow over the upwind part of the dome and the upper part of the cylinder is essentially potential (Frames 5 and 6). However, Frames 6 and 7 clearly show that separation occurs at about 90° - 110°, marking the beginning of the cavity. Frame 8 shows the powerful effect of the background flow in overcoming the secondary flow near the lee surface of the dome. Although a thin haze appears as far upwind as 90°, the main flow in the upper part of the cavity has a strong downwind component which leaves the dome surface radially at an angle of about 150°. The top view shows no lateral spread near the nozzle; in fact the sharp smoke outline through an azimuth angle of 270° indicates that the flow converges toward the nozzle. The side view shows a similar convergence from below.

In Frame 9 the nozzle is partly in the 3-dimensional flow region around the dome and partly in the 2-dimensional region around the cylinder. The flow is upward and laterally outward. Smoke moving upward departs as in Frame 8, but smoke moving laterally outward travels around the sides of the cylinder to the cylindrical separation point near 90°.

In Frame 10 the probe is clearly in the two-dimensional flow zone created by the cylinder. In side view we again see a sharp downwind outline of the smoke cloud near the tip of the nozzle, indicating the strong secondary flow of the cavity vortex impinging on the lee surface of the cylinder. In top view we find an arc of denser smoke hugging the shell.

Frame 11 shows the downwind ground vortex spreading smoke downwind along the ground despite the general reverse flow. Frames 12 and 13 show that the cavity extends at least as far as 2D downwind. In Frame 13 the smoke is indecisive as to direction. Frames 15 and 16 show only downwind flow. It is clear that the cavity boundary is very close to 2.25 D from the shell center.

Generally, we observe that very little smoke is visible downwind of $x \approx 2D$, or higher than $z \approx 1H$ in side view. These may be taken as the effective length and height of the cavity. The maximum total width of the cavity between $x = 0$ and $2D$ is $\approx 1.5D$.

3.23 Gas Diffusion in Non-Uniform Flow Fields

The conventional point-source diffusion equations can not be used for estimating diffusion near objects in a wind stream because they were derived for, and apply only to, uniform flow fields containing straight, parallel streamlines, and homogeneous velocity and turbulence. There are no theoretical solutions available for diffusion in the highly non-uniform flow fields around objects. At the present time, the experimental approach is the only one that shows any promise of providing useful data. The wind tunnel model test is evidently a very practical method of testing a large number of configurations, but data obtained in such tests must be capable of extrapolation to full scale in order to be of use. In this section, we shall describe a procedure for non-dimensionalizing test data for subsequent use on any scale.

In Ref 1, the problems of similarity and scaling are discussed, and it is concluded that diffusion patterns in model and full scale flow fields will be similar if dynamic similarity of the fields exists. Dynamic similarity means that velocities in one flow field can be made to equal the velocities at corresponding points in another flow field by application of a single multiplying factor. In turbulent flow, similarity of instantaneous velocities is not possible, but similarity of mean velocities and the r.m.s. values of the velocity fluctuations are believed to be attainable and adequate for most scaling problems.

To achieve dynamic similarity one must provide geometric and dynamic similarity of the boundary conditions, and Reynolds Number and, sometimes, Froude Number scaling must be used in the flow field. The boundary conditions are, for the most part, controllable. They consist of

a) physical dimensions; including the object, the size, shape and location of the exhaust aperture, and the terrain,

b) velocities; including the mean velocity gradients and turbulence distribution of the background flow, and the mean velocity and turbulence of the effluent at the point of release, and

c) temperatures; including temperature gradients in the background flow and temperature excess of the effluent over the background.

All of the above conditions, except turbulence in the background flow and in the effluent, were controlled during the shell tests. The Reynolds Number was not observed; the Froude Number was observed in the heated surface tests. The effect of these lapses on dynamic similarity will be discussed in a later section. For the present, let us assume that the model and full-scale flow fields have similar mean velocity and turbulence distributions. It follows therefore, that the concentration patterns in the two fields should also be similar.

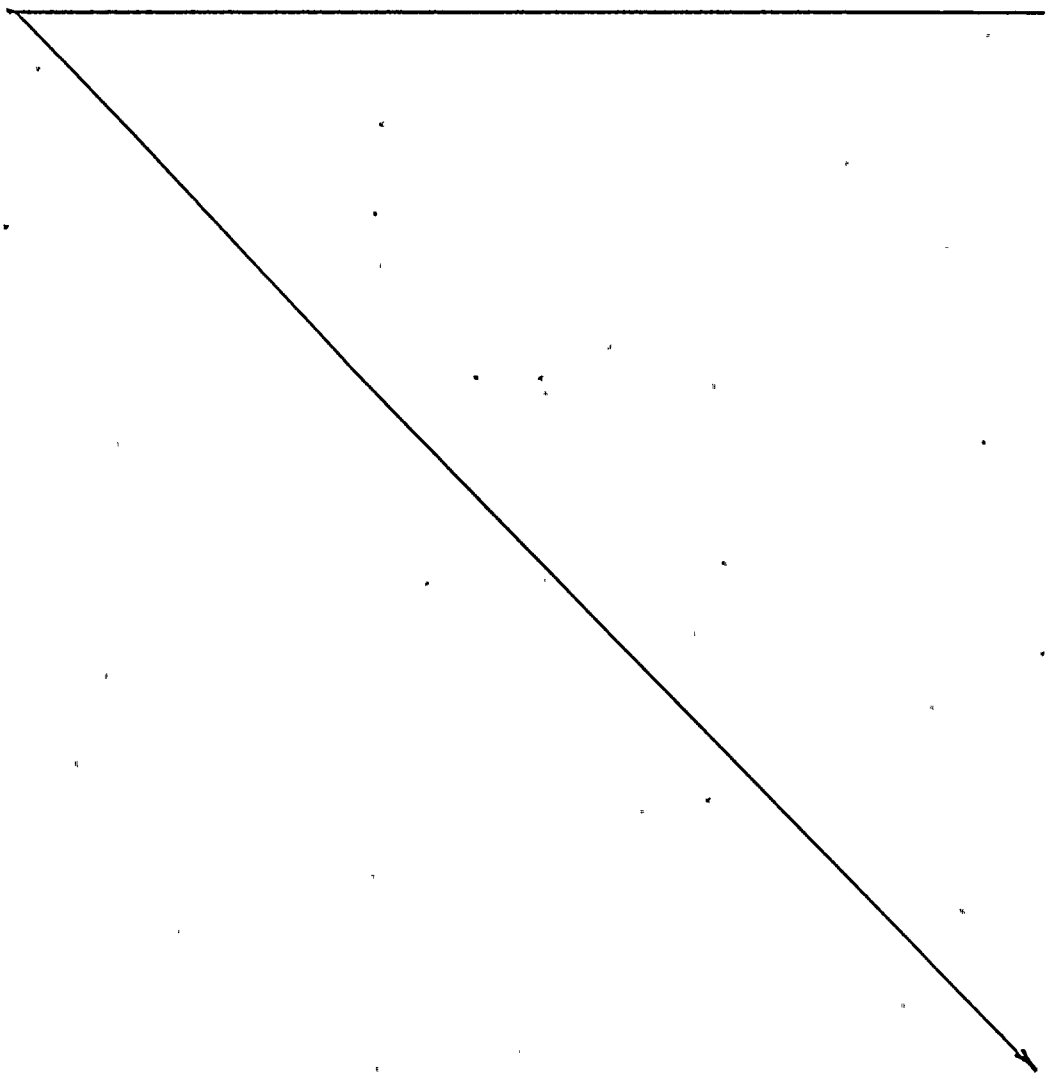

A concentration pattern can be described completely by specifying the local concentration at each point in the field. If two concentration patterns are similar, each should be reducible to the same non-dimensional form by an appropriate scale factor. Let us determine, first, the non-dimensionalizing constants for the simple case of continuous point-source diffusion in a wind stream having uniform mean velocity and isotropic turbulence everywhere. The Hay-Pasquill equation for the special case of linear plume expansion over a short distance, and remoteness from solid boundaries is

$$c = \frac{\dot{Q}}{2\pi \sigma_s^2 V} \exp\left\{ - \frac{r^2}{2\sigma_s^2} \right\} \qquad (3)$$

where: c = gas volume concentration = vol. gas/vol. mixture

$\dot{Q}$ = gas volume release rate (vol./time)

V = uniform mean wind velocity (length/time)

x = downwind distance (length)

σ_s = r.m.s. distance of concentration distribution (length).

If it is assumed that small eddies travel in straight lines for short distances, the concentration distribution can be related to the atmospheric turbulence through the expression

$$\sigma_s = x \sigma_q / V \qquad (4)$$

where: σ_q = r.m.s. velocity fluctuation

Eq (3) then becomes:

$$c = \frac{\dot{Q}}{2\pi (x \sigma_q / V)^2 V} \exp\left\{ - \frac{r^2}{2(x\sigma_q/V)^2} \right\} \qquad (5)$$

Eq (5) can be paraphrased thus:

$$c = \frac{\dot{Q}}{A' V} K' \qquad (6)$$

where:

$$A' = 2\pi (x \sigma_q / V)^2$$

$$K' = \exp\left\{ - r^2 / 2(x \sigma_q / V)^2 \right\}$$

Since K' is an exponential function, it must be non-dimensional, and the argument must also be non-dimensional. Therefore, the non-dimensionalizing length factor must be $\sqrt{2}x\sigma_q/V$. This factor also appears as the radius of a circle of area A', oriented normal to the wind. The quantity $\dot{Q}/A'V$ can then be interpreted as an average concentration produced by depositing Q of gas into a duct of cross-section area A' carrying an air stream of uniform mean velocity V:

$$c_{av} = \dot{Q}/A'V \tag{7}$$

From Eqs (6) and (7), we can write

$$K' = c/c_{av}, \tag{8}$$

and the non-dimensionalizing factor for concentrations becomes $c_{av} = \dot{Q}/2\pi(x\sigma_q/V)^2V$.

The quantity c_{av} determines the general magnitude of the concentrations and, therefore, it may be said to define the scale of the problem. The quantity K' simply describes the relative magnitudes of the concentrations in the field, independent of scale. It will be called the distribution function. K' is wholly dependent on the coordinates x and r, and the dynamic property σ_q/V, assumed uniform everywhere in the flow field. The uniformity of σ_q/V automatically provides dynamic similarity in all fields to which Eq (5) applies.

We now wish to apply the same type of reasoning to diffusion in the non-uniform, non-homogeneous flow field about an object. Unfortunately, no theoretical solution for the concentration distribution is available. However, we have specified that the mean velocity and turbulence distributions in model and full scale are similar. Therefore, we may expect that an equation similar to Eq (6) can be written, containing a scale term $\dot{Q}/AU$ and a distribution function K:

$$c = \frac{\dot{Q}}{AU} K \tag{9}$$

In Eq (9), c and $\dot{Q}$ have exactly the same meaning as in Eq(6), but A, U and K are analogous to, but not the same as, A', V and K'. The difference lies in the fact that A', V and K' for a uniform field are uniquely defined, whereas A, U and K in a non-uniform field are not. Nevertheless, Eq (9) can be made to serve the same function as Eq (6) by arbitrarily selecting an area A and a velocity U in the flow field, and calculating K at each point in the field using experimental determinations of c for a gas release rate $\dot{Q}$. By measuring c and calculating K at a sufficient number of points, the function K can be determined in the entire flow field. In this procedure, the numerical value of K is meaningless without a statment as to how A and U are to be measured, but once this

statement is made, K is as firmly established as K'. Evidently, the functional form of K will not be affected by the arbitrary choice of the constant AU, although the magnitude will. In the present tests, U was taken as the mean wind velocity at an elevation of 160 ft (20 inches in the tunnel). The area A was chosen as the cross-section area of a projection of the shell in a plane transverse to the mean wind direction. The area choice was suggested by the concept of an average concentration in the wake equal to $c_{av} = Q/AU$, analogous to Eq (7).

In some of its properties, K resembles the lift and drag coefficients used in aerodynamics, and the friction factor used in hydraulics. It is a non-dimensional coefficient which maintains a more or less constant magnitude over a wide range of values of the independent parameters to which it is related. One important difference between K and a lift coefficient, however, is that K is not a single-valued quantity for a total configuration, as C_L is for a given airfoil shape. K varies from point to point in space and must be viewed as a field: $K = K(x/L, y/L, z/L)$, where x, y and z are space coordinates and L is a reference length. However, each dynamic configuration has a unique K field which is independent of the magnitude of $\dot{Q}$, U and A. K values in the field are, of course, time-means.

3.24 K-Isopleths

The value of K at each sample point was calculated according to the formula:

$$K = \frac{1.7\, c_m A_m U_m}{\dot{Q}_m} \qquad (10)$$

where: c_m = sample volume concentration (ppm)

A_m = shell frontally projected area = 0.776 ft^2

U_m = mean wind velocity (ft/sec) at Z_m = 20 inches

$\dot{Q}_m$ = gas release rate (cc/min)

$_m$ = subscript to designate "model"

The point values were then plotted on graphs corresponding to a surveyed plane, and isopleths of constant K were drawn through the points. The results are presented in Figs 8 to 36. Each Figure represents a different configuration. The tests will be discussed in groups, following their arrangement in Tables 1 and 2.

Figs 8 - 14

This series is the most comprehensive in the program. The basic configuration is the shell alone at ambient temperature in an isothermal wind having a logarithmic velocity profile. The variable is the source location. The isopleths of Figs 8 - 12 may be compared with the photographs of Fig 6 as follows:

Release point	bottom upwind	mid-height upwind	top	mid-height downwind	bottom downwind
Isopleth Fig No.	8	9	10	11	12
Photograph 6, Frame No.:	2	5	7	9	11

Each Figure contains isopleths in the longitudinal centerplane, in a horizontal plane 4 ft above ground, in transverse planes at X/D=1.25 and 2.5, and along the shell surface.

Fig 8, bottom upwind release, is characterized by the splitting of the gas into two highly concentrated symmetrical streams moving downwind along the base of the shell and separating near $\Theta = 90^{\circ}$. After the streams leave the shell, the line of maximum concentration appears to follow the cavity outline at a lateral distance of $\sim$ D/2 from the axis. However, gas is found along the ground up to $\sim$D/2 upwind and $\sim$D laterally from the base of the shell. This is believed to have been caused by the upwind ground vortex. Vertical diffusion is negligible along the upwind shell surface, but diffusion in the cavity causes contamination of the entire lee surface of the shell.

In Fig 9, mid-height upwind release, the air flow near the release point is principally in the upward and lateral directions, producing strong contamination of the upwind dome surface and general contamination of the entire lee surface of the shell. The upwind cylindrical surface is not contaminated. Gas concentrations in the cavity are highest near the top.

Fig 10, top release, is similar to Fig 9, except that the upwind dome surface is clear.

Fig 11, mid-height downwind release, shows high concentrations along the lee surface of the dome and in the top of the cavity. Ground concentrations are about the same as in Figs 9 and 10.

Fig 12, bottom downwind release, shows high concentrations along the lee surface of the shell from ground to mid-height, and high ground concentrations in the cavity for a distance of $\sim$ D from the base of the shell.

Fig 13, bottom side release, shows an asymmetric pattern with high concentrations near the release point, of the same order of magnitude as in the symmetrical bottom upwind release of Fig 8. The high ground concentrations are found closer to the axis than in Fig 8.

Fig 14, mid-height side release, shows low ground concentrations everywhere in the cavity. Apparently the gas stream separates from the side of the shell and undergoes considerable diffusion before joining the secondary flow. There appears to be some indication of a local high concentration region near the top of the dome on the side opposite the release point.

It is of some interest to determine the maximum concentration in the vicinity of the shell as a function of distance from the shell. Such curves are shown in Fig 37, based on the data of Figs 8 - 13. The abscissa S/D is a non-dimensional straight line distance from the shell surface to the farthest point of a given K isopleth, measured as shown in the sketch. The numerals on the curves designate the Figure Number. The letters C and G indicate whether the maximum value of K was found within the cavity or on the ground, respectively. The heavy dashed line approximates the maximum value of K measured in these configurations at the distance S/D. The line may be expressed by the formula

$$K_{max} = \frac{20}{(S/D)^2} \qquad (11)$$

Maximum concentrations occur at the ground for bottom release points, and in the cavity space for mid-height and top release points. The maximum ground and cavity concentrations are about equal. The bottom upwind and bottom side releases are critical for ground contamination. The mid-height downwind release is critical for cavity contamination.

Figs 15 - 17

These tests were made to determine the effect of wind velocity profile on concentrations in the longitudinal centerplane of the cavity. The following configurations are comparable except for profile:

Release point:	bottom upwind	top	bottom downwind
Log Profile Fig No.:	8	10	12
Uniform Profile Fig No.:	15	16	17

There is very little difference in the K isopleths for the top release. The bottom upwind release is affected markedly, concentrations in a uniform profile being less than in a logarithmic profile everywhere in the cavity by a factor of 4 or more. The bottom downwind release is affected to a lesser degree, the concentrations being lower by a factor of ~ 1.5.

Figs 18 - 20

These tests were made to check the effect of Reynolds Number by varying the wind velocity. The tests were run only with a uniform profile. Isopleths may be compared to Fig 16.

The shapes of the isopleths in the longitudinal centerplane of the cavity do not change much as the wind velocity is varied from 3 to 15 ft/sec. The variation of maximum concentration with distance is shown

in Fig 38, with wind velocity as a parameter. K is found to reduce by a factor of 2 over the tested velocity range, the bulk of the reduction occurring in the step from 10 to 15 ft/sec. It is not clear from the data whether this is a Reynolds Number effect or experimental error.

Figs 21 to 23

These tests were made to evaluate the effect of heating the shell surface. Customarily, tests involving elevated temperature are run with Froude Number scaling, which requires that the velocity be reduced by a factor equal to the square root of the linear scale. Thus, the velocity scale factor is $\sqrt{96} = 9.22$ and the reference velocity $= U_m = 16.7/9.22 = 1.8$ ft/sec. The tests were actually run at 1.7 ft/sec.

Fig 21 may be compared with Fig 10 to observe the effect of reducing the absolute wind velocity while maintaining a logarithmic profile. In Fig 21, the isopleths between the shell surface and X/D = 1.5 are believed to have been based on questionable test data, and should be ignored. At distances greater than X/D = 1.5, the isopleths for $U_m = 1.7$ ft/sec appear to be smaller than those at 5.54 ft/sec by a factor of about 2. This is contrary to the trend shown in Figs 18 - 20. Actually, insufficient data were taken to draw detailed isopleths at 1.7 ft/sec; therefore Fig 21 will be disregarded; Fig 10 will be taken as representative of the isopleth pattern at a temperature differential of 0°F.

When the surface temperature is raised to 150° F above ambient (Fig 22), the limited data indicate that convection currents created by heat loss from the shell carry most of the gas stream out of the cavity, and produce only very small concentrations on the ground and at the shell surface. At a differential of 300°F, none of the gas reaches the ground.

Figs 24 to 28

As seen in Frame 4 of Fig 6, the concentrations around the shell are affected strongly by the presence of upwind auxiliary buildings. These buildings create their own displacement fields, cavities and wakes, which, in effect, become the background flow for the shell. In SW and SSW winds, the principal upwind building is the 40 ft high, L-shaped power plant. The lower part of the 98 ft high shell is immersed in the wake of the power plant. The upper part is exposed to the normal background flow.

The general flow pattern at low elevations is very complicated. It consists, roughly, of two elements: one is a characteristic cavity vortex between the power plant and the shell; the other is a smooth air stream that splits laterally around the power plant, the westerly branch swinging around the edge of the building and being diverted toward the shell by the 46 ft high sodium boiler building to the North. This westerly branch impinges on the shell, flows around it, and leaves the shell vicinity through the NE passage between the sodium boiler building and the fuel cycle facility (16 ft high).

In Figs 24 to 28, the isopleths are in a horizontal plane 4 ft above the ground; the x-marks are individual sample locations on the building roofs. In Fig 24, bottom upwind release, most of the gas is caught in the power plant cavity, some of it even moving upwind over the power plant roof. Generally, the concentrations between the shell and the power plant are higher than the concentrations downwind of the shell.

In Fig 25, top release, the gas concentration pattern on the ground is similar to the pattern around a chimney. There are little or no concentrations at the base of the shell, and the maximum concentration is in the vicinity of 5D downwind. This condition is caused by the channeling of air into the shell cavity by the sodium boiler and fuel cycle buildings, partially destroying the shell cavity vortex and reducing downwash and secondary flow.

In Fig 26, mid-height downwind release, conditions are about the same as in Fig 24.

In Fig 27, bottom downwind release, the release point is in the partial shell cavity, and fairly high concentrations are found downwind of the shell.

Fig 28 shows the worst configuration with respect to contamination of the region upwind of the shell. It occurs in a SSW wind. It is interesting to note that the values of K = 8 and 10 on top of the power plant are found at distances that satisfy Eq (11). For example, $S/D=\sqrt{20/10}=1.4$ at K=10.

Figs 29 to 32

These figures show the effect of the presence of the shell on the concentration downwind of a stack whose height is equal to the shell height. The wind and stack parameters were maintained constant for all four tests. The wind contained the standard logarithmic velocity profile; its mean velocity at the elevation of the stack opening was 5.2 ft/sec. The effluent was discharged at a velocity of 4.6 ft/sec. The effluent/wind velocity ratio was 0.9 at the stack opening. The variable was the location of the shell; it was placed in several locations with its center 1H or 98 ft from the center of the stack.

The configurations may be evaluated by comparing the maximum ground concentrations, summarized in the following table:

Fig No.:	29	30	31	32
Shell location:	none	side	downwind	upwind
K_{max} at ground:	0.01	0.1?	0.35	0.7
X/H at K_{max}:	17	20?	12	7

The greatest ground contamination occurs with the upwind shell location, K_{max} being 70 times greater than for the stack alone. This is explainable by noting that the stack aperture is located approximately on the cavity boundary, whose streamlines curve downward, carrying the effluent to the ground with a minimum of dilution (see sketch on Page 9).

When the shell is downwind of the stack, the aperture is in the displacement flow, and the effluent is carried over the cavity, descending farther downwind and at the same time, experiencing greater dilution. The increase of 35 times in K_{max} over the stack alone condition is only half as much as in the upwind shell location, but it is still considerable.

The side location of the shell produces a maximum ground concentration 10 times as high as the stack alone. The question marks in the table indicate that these measurements, taken in a longitudinal plane through the stack, may not be true maxima, since the streamlines passing through the region near the stack opening take on a lateral curvature and may descend to the ground with higher concentrations at some lateral distance from the centerline.

In interpreting these results with respect to full-scale conditions, it must be noted that the full-scale exhaust velocity is 35 mph (51 ft/sec), and therefore, the corresponding full-scale wind velocity at the top of the stack must be 35/0.9 = 39 mph. A smaller wind velocity will create a higher effluent/wind velocity ratio, which will raise the plume to the top, or out, of the cavity, and reduce ground concentrations.

Figs 33 to 36

These tests were similar to the previous series except that the stack height was increased 50%. The stack opening was, therefore, well above the cavity for all locations of the shell. In comparing the configurations, we are not able to use K_{max} at the ground as in the previous series, since K_{max} occurs farther downwind than the observations. For convenience, we shall use K at X/H = 17, Z/H = 0.2. The following table summarizes the results:

Fig No.:	33	34	35	36
Shell location:	none	side	downwind	upwind
K [17,0.2]:	0.004	0.002?	0.05	0.18

K at this point is increased by a factor of 45 for the upwind shell and 12 for the downwind shell. The results for the side location of the shell must be regarded, again, as uncertain.

4. EVALUATION OF RESULTS

The calculation of diffusion may be regarded as a two-part process; one is the establishment of an average concentration in the field, the other is the determination of a function that describes the variation of concentration from point to point in the field. The former quantity is specified, for continuous gas release in a moving air stream, by the gas release rate, the wind velocity, and some representative area. There is no ambiguity in these terms, and they need no evaluation. The latter quantity, called the distribution function, appears to be wholly dependent upon the mean and turbulent velocities of the flow field. If the distribution function is found, either analytically or experimentally, for one flow field, then the same function will apply to all dynamically similar fields. The evaluation of the test results, therefore, need concern itself only with the distribution function and the nature of the flow field to which it applies.

In distorted flow fields, such as occur around objects in a wind stream, the distribution function K is determined experimentally by a series of simple measurements and a simple calculation. The precision of the measurements is far greater than the concentration variation with time at any given point, and so we may assume that the principal error in measurements would appear in the estimation of the mean concentration from a record that shows very high fluctuations at many points in the field. It is believed that the resulting maximum error in K is no greater than 10% for any individual sample determination. However, the unsteadiness of flow around objects, particularly the long period fluctuations, may give rise to variations of up to 25% in the K determinations for groups of points. This effect is noticed mostly in regions where the concentration gradients are high.

The characterization of the flow field that exists during the determination of a set of K-isopleths is more of a problem. The classical hydrodynamic treatment of isothermal, viscous, non-turbulent flow leads to the conclusion that, if the boundary conditions and Reynolds Number are specified, the flow field is also specified, even if an analytical solution of the equations of motion can not be obtained. In non-turbulent flow, the boundary conditions are zero velocity at all solid surfaces and a prescribed velocity variation at large distances from the source of disturbance, in this case the shell. Generally, these conditions can be met, although the Reynolds Number would have to be very low to produce completely laminar flow.

Reynolds Numbers encountered in model testing and in full-scale are always higher than the critical Reynolds Number for the onset of turbulence, and turbulence is always present in the flow field. There are two sources of turbulence, however. One is the turbulence in the background flow and the other is the turbulence in the wake downwind of an object. The relationship between the two has not been clearly established. Wake turbulence will occur at a high enough Reynolds Number even if the background flow is laminar, but a turbulent background flow induces wake turbulence at a lower Reynolds Number. Clearly, the boundary conditions for turbulent flow must include the distribution of turbulence as well as mean velocity in the background flow.

Assuming that the turbulent background flow boundary conditions are met, we must now evaluate how the Reynolds Number affects the flow field, if we wish to estimate its effect on K. When the Navier-Stokes equations of fluid motion are non-dimensionalized, it is found that the inverse of the Reynolds Number appears as a coefficient of the shear stress term. Thus, if shear stresses are absent, Reynolds Number will not be relevant, and if Reynolds Number is high, the shear term will be numerically small; in either case, the shear term may be neglected. This leaves the Navier-Stokes equations devoid of any scaling parameter, and the flow pattern becomes potential and independent of scale. We conclude, therefore, that Reynolds Number scaling is important wherever shear stresses are high. Since shear stresses are proportional to velocity gradients, we may expect that Reynolds Number effects will show up in the boundary layer, and in those regions that are controlled by boundary layer activity.

It has been found that the boundary layer thickness on a surface of finite length varies inversely as the Reynolds Number. Therefore, we may expect that boundary layers on the full-scale shell will be proportionately thinner than on the model. Reduction in boundary layer thickness is equivalent to an increase in velocity at the same distance from the surface. Consequently, ventilation is greater, and gas concentrations should be smaller. An indication of this was found in the uniform profile tests, Figs 15 to 17, where the boundary layer of the background flow was only 4 inches thick, compared to the logarithmic profile boundary layer that occupied the entire tunnel height.

The important role of the boundary layer in the formation of the wake and cavity was described in Section 3.21. It was shown that the size of the cavity depends strongly on the location of the line of separation, which, in turn, depends on the energy in the boundary layer. High Reynolds Number flows have thin, high-energy boundary layers which tend to remain attached to rounded surfaces. Therefore, the line of separation moves downwind as Reynolds Number is increased, and the cavity size decreases.

The effect of increasing the energy in a boundary layer by introducing a disturbance at the surface, and thereby replacing low energy air from the boundary layer with high energy air from the potential flow, is shown in Fig 7. The photographs at the right were made with the shell in the normal test configuration. The photographs at the left were made with a $\frac{1}{4}'' \times \frac{1}{4}''$ angle taped to the surface of the shell with its outstanding leg along $\Theta = -45^{\circ}$. The angle, or tripper, causes the boundary layer to separate farther downwind, as seen in side elevation. The half-width of the cavity on the tripper side (upper left photograph) is seen to be somewhat smaller than in the other configurations, and the cavity boundary appears to be sharper.

If gas is released in the cavity, the available air volume for dilution is reduced, and concentrations within the cavity should increase. However, gases released outside the cavity should have a greater chance to dilute.

These considerations are, of course, qualitative. Unfortunately, no experimental data are available at present to evaluate the net effect of

background turbulence and Reynolds Number on concentrations in the cavity. Research on this aspect is now in progress (Ref 2). However, we would like to call the reader's attention to several correlation studies which bear upon, and tend to confirm, the above line on reasoning, although they can not be cited as conclusive evidence.

Refs 3 and 4 are a correlation study of wind tunnel and full-scale tests of gas released in the streets of a model city. The results of both phases were non-dimensionalized in a manner similar to the one used in this report (although the reference area A was selected differently), and the distribution functions found in the two phases were in reasonable agreement.

Ref 5 compares pressure differences on a model and a full-scale building in a wind stream. It was found that the pressure pattern on the building could be duplicated only when the atmospheric mean velocity profile was reproduced in the tunnel. The similarity of pressure patterns indicates that the velocity fields outside the boundary layer were probably quite similar. If diffusion depends only on the velocity field, then the requirement for uniqueness of a K field would demand scaling of the mean velocity of the background flow.

Ref 6 is the often-cited Rock of Gilbraltar study. The full-scale flow field was studied by balloon tracking and observations of cloud formation. The tunnel flow field was studied by visual observation of threads attached to wires. It was concluded that qualitatively, at least, the flow fields in the lee of the mountain were similar as to mean velocity and turbulence distribution.

In summary, it is believed that the K-isopleth patterns presented in this report are basically independent of scale, but will be subject to some variation as a result of changes in Reynolds Number and turbulence in the background flow. Sensitivity to these variables is attributed to the rounded surface of the shell, which permits movement of the separation line and, therefore, variation of the cavity size. This condition does not exist for buildings with sharp edges, since the separation line is fixed at the edges for all Reynolds Numbers (see Ref 1).

To some extent an increase of turbulence and an increase of Reynolds Number have opposite effects, the former providing greater dilution by eddy activity, and the latter providing less dilution due to shrinkage of the cavity. The net effect is unknown. The tunnel turbulence during the test was not measured, but subsequent measurements in flows produced by a grid of 2-inch wide slats on 6-inch centers plus a length of very rough terrain, produced an average value of turbulence intensity $\sigma_q/V = 10\%$. It is believed that a similar value was achieved during the shell test series. For comparison, the turbulence intensity in the empty tunnel is of the order of 0.1%.

One aspect of diffusion scaling, that sometimes is not given due attention, is the implicit assumption that the flow field is independent of the source strength $\dot{Q}$. This is true when the gas molecules merely replace air molecules in the effluent, and the total velocity of emission is

unchanged. Evidently, this condition can be achieved only if the gas concentration in the effluent is less than 1. When pure gas is released from a fixed aperture, the emission velocity will vary with $\dot{Q}$ and a new flow configuration will be established for each value of $\dot{Q}$. The K-field will be very sensitive to $\dot{Q}$ in a small region close to the emission aperture, but the sensitivity decreases rapidly with distance. This is the justification for use of the point-source equations in stack diffusion calculations, and the reason for the lack of validity of these equations close to the source. In the present test series, the gas release rate for measurements near the source produced a negligible emission velocity ($V_e \approx 0.2$ ft/sec). The high release rate ($V_e = 8$ ft/sec) was used only for measurements at large distances from the shell. Effectively then, the shell releases can be properly classified as "leaks". In the stack tests, the gas concentrations in the effluent were too small to noticeably affect the effluent velocity.

5. APPLICATION TO FULL SCALE DIFFUSION CALCULATIONS

If exact dynamic similarity of a model and a full-scale configuration can be found, the full-scale concentration may be calculated by:

$$c_f = \frac{\dot{Q}_f}{1.7\ A_f U_f} K \qquad (12)$$

where:

c_f = concentration (ppm)

A_f = shell frontally projected area = 7160 ft^2

U_f = mean wind velocity(ft/sec)at Z_f= 160 ft

$\dot{Q}_f$ = gas release rate (cc/min)

$_f$ = subscript to denote full scale.

The factor 1.7 may be omitted if Q_f, A_f and V_f are in consistent units and C_f is dimensionless. The value of K at any point [X/D, Y/D, Z/D] may be taken from the appropriate Figure. The formula may be modified by the introduction of a numerical constant if the velocity at a different reference elevation is used.

In practical situations, one is often interested in determining the horizontal distance from the base of a shell, within which the concentrations will be higher than a given value, irrespective of the location of a leak in the shell. Eq (11) is suitable for such estimates. Substituting (11) into (9), we derive

$$c = \frac{\dot{Q}}{AU} \cdot \frac{20}{(S/D)^2}, \qquad (13)$$

or, since in this case, $A = 1.12\ D^2$,

$$S = 4.2\sqrt{\dot{Q}/Uc_{allow}} \qquad (14)$$

where S, $\dot{Q}$, U and c_{allow} are in consistent units.

Eq (14) produces conservative values of S, since the numerical constant 20 in Eq (11) was taken high enough to include all test data. From Fig 37, one may see that a numerical constant of 10 would be a better average fit for the test data. If the average fit is acceptable, the coefficient of Eq (14) should be reduced to $4.2/\sqrt{2} = 3.0$.

When gas is released on the upwind face of the shell, the primary flow carries a concentrated gas stream downwind along the cavity surface toward stagnation point C, where the gas stream splits, part moving downwind and part moving toward the shell in the secondary flow. Thus, the

downwind face of the shell is bathed in a contaminated stream whose base concentration can not be less than the concentration at point C. We may estimate K at point C, since we have found that the cavity length is X/D = 2.25 measured from the center of the shell, or S/D = 1.75 measured from the shell surface. Therefore K at point C $\approx 10/1.75^2 \approx 3$. An examination of the Figures shows that an average value of K along the downwind part of the cylindrical face of the shell is also about 3 for top, upwind and side releases.

Downwind of the cavity, the flow field first acquires the wake velocity profile and then the background flow profile. It would be convenient to be able to compute a continuous maximum ground concentration through all these regions, starting from the shell surface.

At large distances from a continuous point source at ground level, the maximum concentration at ground level may be expressed by

$$c = \frac{\dot{Q}}{\pi \sigma_y \sigma_z V} \quad \text{(see Ref 7, sec 5.3)} \tag{15}$$

and

$$\sigma_y = x\sigma_\theta = x(\sigma_v/V)$$

$$\sigma_z = x\sigma_\theta/2 = x(\sigma_v/V)/2$$

where

σ_θ is the lateral r.m.s. gust angle

σ_v is the lateral r.m.s. fluctuation velocity

The recommended value of σ_θ for a neutral atmosphere is given as a function of distance from the source, as follows:

x (feet):	330	990	1980	3300
σ_θ (radians):	.076	.065	.056	.049

Expressing Eq (15) in terms of σ_θ, we have

$$c = \frac{0.64\dot{Q}}{x^2 \sigma_\theta^2 V} \quad \text{for} \quad x > 330 \text{ ft} \tag{16}$$

We may transform the empirical Eq (13) into the form of Eq (16) by using $A = 1.12D^2$, and a numerical constant of 10 instead of 20, in which case,

$$c = \frac{\dot{Q}}{1.12D^2 V} \cdot \frac{10D^2}{S^2} = \frac{8.9\dot{Q}}{S^2 V} \text{ for } S/D < 5 \tag{17}$$

Eq (16) will predict the same concentration as Eq (17) if $s = x$ and $\sigma_\theta = 0.27$. Therefore we find that the rate of diffusion for at least 2 cavity lengths downwind of the shell is about 4 times the rate in a neutral atmosphere ($\sigma_\theta \approx 0.07$).

The transition from cavity turbulence to normal turbulence in the atmospheric boundary layer depends on the rate of decay of the wake. Experiments with flat plates normal to a laminar air stream in a wind tunnel show that the wake is quite persistent, having been measured as far as 680 disk diameters downwind, and that the turbulence decreases as $(x/d)^{-2/3}$ for the range $10 < x/d < 1000$. The -2/3 law may also be predicted from momentum considerations. For lack of better data, we suggest the use of the following values of σ_θ in conjunction with Eq (16) for the calculation of diffusion in wakes in the atmosphere:

for $0 < S/D < 5$, σ_θ = constant at 0.27

for $5 < S/D < 40$, $\sigma_\theta = 0.8\ (S/D)^{-2/3}$

for $40 < S/D$, σ_θ = constant at 0.06

These values conform to our measurements close to the shell, to the Hay-Pasquill suggested values at large distances and to the theoretical (and experimentally confirmed) variation between the cut-off levels.

6. RECOMMENDATIONS

The concentration measurements made during this study have been reduced to a non-dimensional coefficient form designated by the symbol K. As such, they are believed to be independent of scale in the same context that the aerodynamic drag coefficient C_D and the hydraulic friction factor f are independent of scale. Practically, this means that the coefficients are not absolutely constant over a range of scales, but are sufficiently so to allow order of magnitude estimates in most of the range. Evidently, more precise estimates require knowledge of the variability of the coefficients.

Under the pressure of engineering economics, considerable effort has been expended in the study of the aerodynamic and hydraulic coefficients; their nature and variability is now well-understood and well-documented. On the other hand, very little is known about the concentration coefficient K. Research in atmospheric diffusion from 1915 to 1945 was done primarily in response to military demands, and was directed toward the solution of simple diffusion problems in uniform flows. Those important studies led to formulas involving diffusion coefficients, of which a number have been, and still are being, suggested. Since 1945, attention has turned from military needs to environmental sanitation, and the focus is now on the very numerous sources of contamination near industrial buildings. However, the classic solutions are not valid for the distorted flow fields near such buildings, and a more generalized form of the diffusion coefficients is required. The concentration coefficient $K = K[x,y,z]$ is a general coefficient of this type.

There is ample room for research into the nature of K and its dependence on known and, as yet unknown, parameters. Two types of information are required: one is the delineation of K distribution patterns around buildings or groups of buildings other than the prisms of Ref 1 or the shell of this report; the other is a study of the variation of these patterns with Reynolds Number, Froude Number and atmospheric turbulence, at the least. The former may be carried out most conveniently in the wind tunnel, the latter will require some tests in the full-scale atmosphere. The two studies are not disjoint, since proper wind tunnel procedure will depend on precise knowledge of the circumstances under which certain scaling procedures are mandatory.

Taking into consideration the need for more order-of-magnitude data, the uncertainty of extrapolation procedures and the available test facilities, it would appear that two avenues of research should be pursued. Some full-scale studies should be made at the EBRII site to determine whether the K-isopleths found in the tunnel are in reasonable agreement with field studies, and model studies of diffusion in built-up areas should be undertaken. The EBRII study would supplement the correlation research now in progress (Ref 2) by introducing a rounded building configuration and extending the range of Reynolds Number. The built-up area study would be more representative of practical configurations. The EBRII complex would be ideal as a prototype built-up area for gas released from sources located on buildings or at various stack elevations.

REFERENCES

1. Halitsky, J., 1963: Gas Diffusion Near Buildings. N.Y.U. Dep't. of Met. and Ocean., Geophys. Sci. Lab. Rept. No. 63-3.

2. U.S.P.H.S. Research Grant No. AP-59(R1) to James Halitsky at New York University, 1962: Effect of Turbulence on Gas Diffusion Near Obstacles.

3. Kalinske, A. A., Jensen, R. A. and Schadt, C. F., 1945: Wind Tunnel Studies of Gas Diffusion in a Typical Japanese Urban District. OSRD, NDRC, Div. 10 Informal Rep. No. 10.3A-48, available from Library of Congress, Wash., D. C.

4. Kalinske, A. A., Jensen, R. A. and Schadt, 1945: Correlation of Wind Tunnel Studies with Field Measurements of Gas Diffusion. OSRD, NDRC, Div. 10 Informal Rep. No. 10.3A-48a, available from Library of Congress, Wash., D. C.

5. Jensen, M. 1958: The Model-Law for Phenomena in Natural Wind. Ingeniøren 2, Dansk Ingeniørforening. Denmark. pp 121-128

6. Field, J. H. and Warden, R., 1933: A Survey of the Air Currents in the Bay of Gibraltar, 1929-30. Air Ministry, Geophys. Mem. No. 59, London.

7. Pasquill, F., 1962: Atmospheric Diffusion. D. Van Nostrand Co., London, 297 pp.

TABLE 1. SUMMARY OF SHELL RELEASE TESTS

Fig.No. of Test Results	Model					Wind		
	Configuration	Surf.Temp. Diff., °F	Gas Release Loc. X/D	Y/D	Z/D	Ref.Vel. ft/sec	Profile	Direction
8	Shell	0	-1	0	0.07	5.54	Log.	
9	Alone		-1	0	0.78			
10			0	0	1.22			
11			1	0	0.78			
12			1	0	0.07			
13			0	-1	0.07			
14			0	-1	0.78			
15		0	-1	0	0.07	5.54	Uniform	
16			0	0	1.22			
17			+1	0	0.07			
18		0	0	0	1.22	3	Uniform	
19						10		
20						15		
21		+0	0	0	1.22	1.70	Log.	
22		+150						
23		+300						
24	Shell	0	-1	0	0.07	5.54	Log.	SW
25	and		0	0	1.22			SW
26	Auxiliary		1	0	0.78			SW
27	Buildings		1	0	0.07			SW
28			-1	0	0.07			SSW

D = Reactor shell diameter = 80 ft

TABLE 2. SUMMARY OF STACK RELEASE TESTS

Fig.No. of Test Results	Configuration		Wind	
	Stack Height	Reactor Location	Ref. Vel. ft/sec.	Profile
29	1H	none	5.54	Log.
30		1H to side		
31		1H downwind		
32		1H upwind		
33	1.5H	none	5.54	Log.
34		1H to side		
35		1H downwind		
36		1H upwind		

H = Reactor shell height = 98 ft

TABLE 3. SHELL SURFACE TEMPERATURE EXCESS ABOVE TUNNEL AMBIENT TEMPERATURE

Location	Temperature Excess, °F	
	Test Fig 22	Test Fig 23
Dome upwind	185	373
Dome downwind	188	371
Cylinder upwind	119	241
Cylinder downwind	115	233
Average	152	304

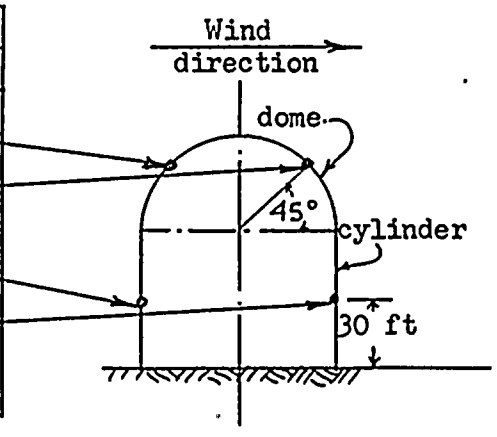

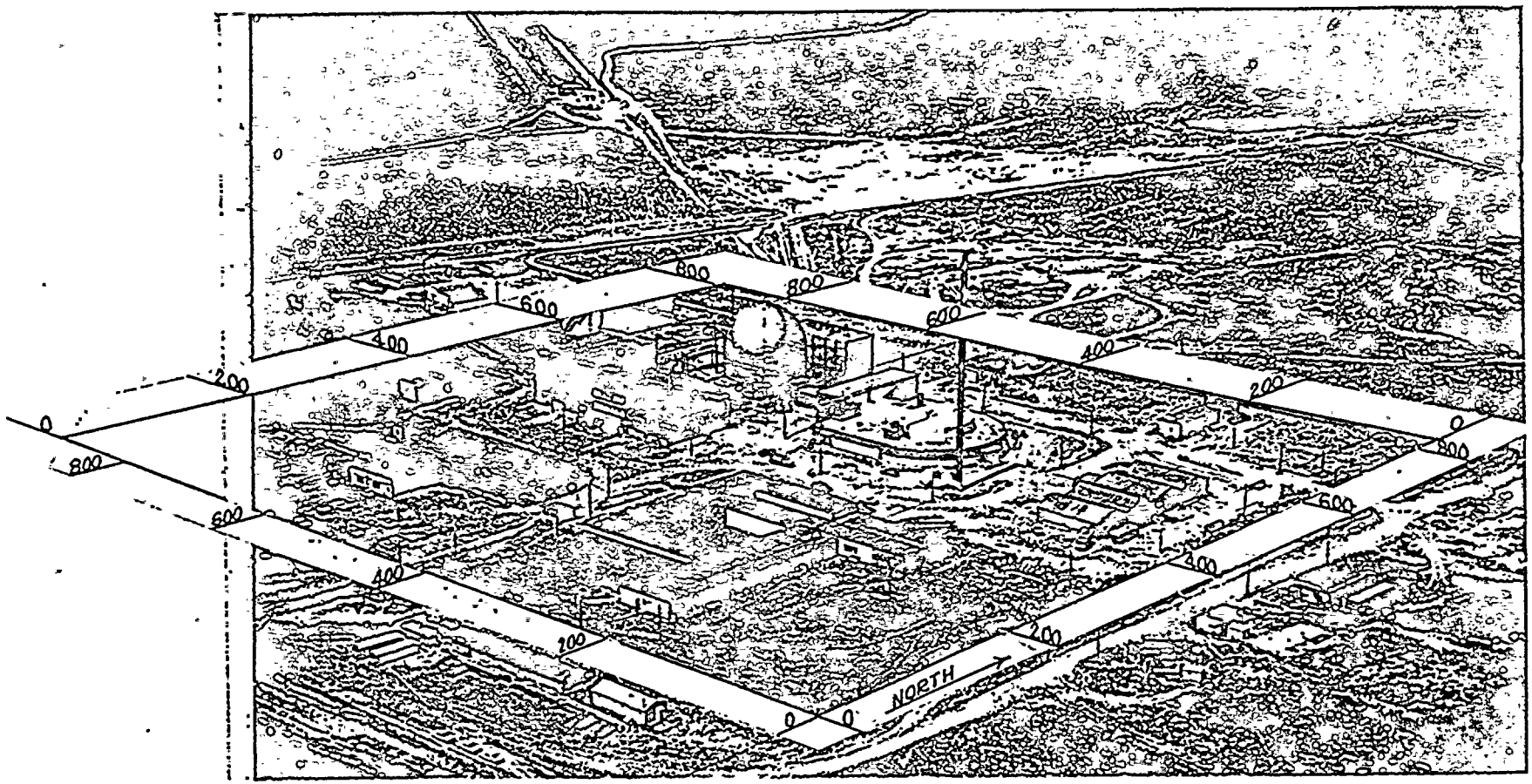

Fig. 1 Photograph of NRTS Complex

Dimensions are distances in feet

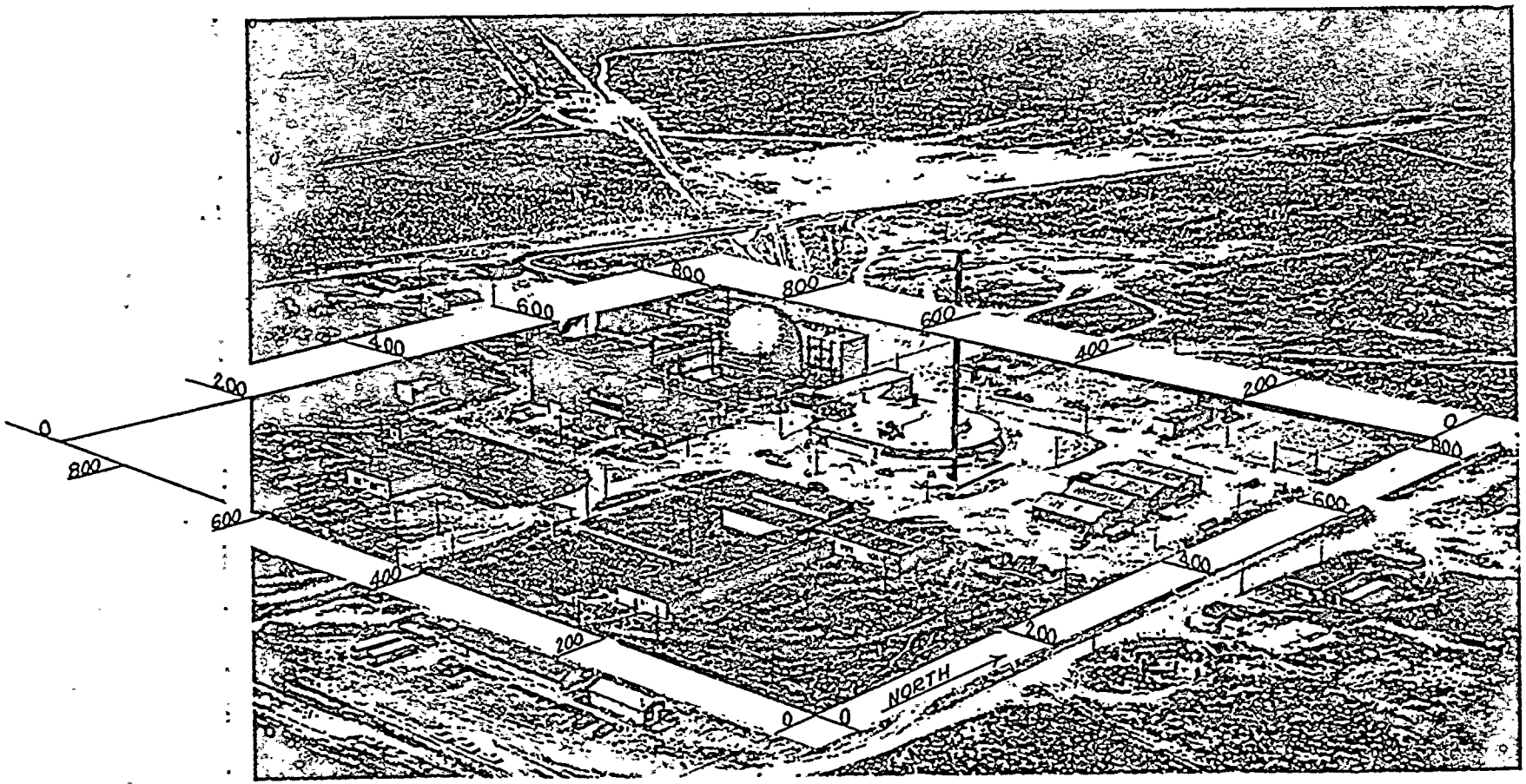

Fig. 1 Photograph of NRTS Complex

Dimensions are distances in feet

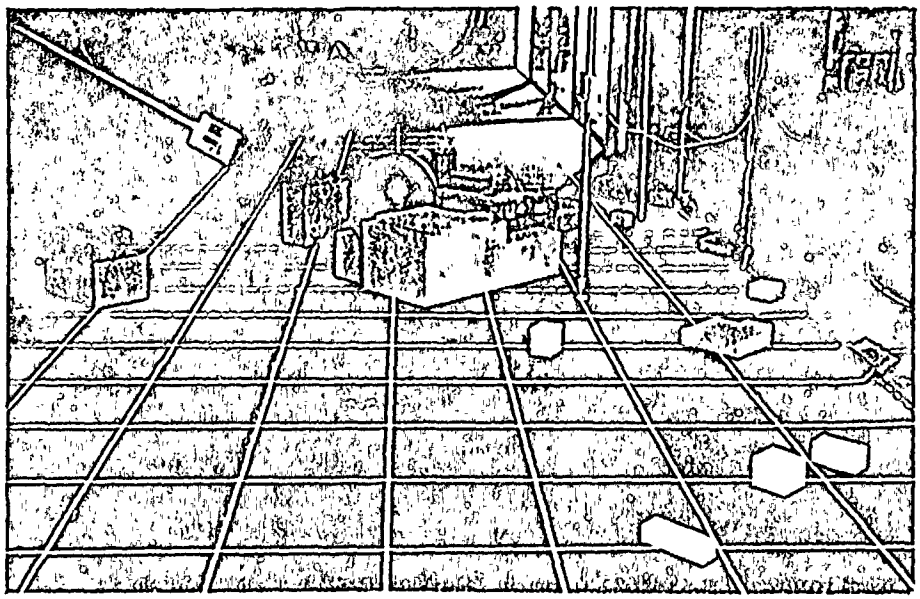

looking downwind

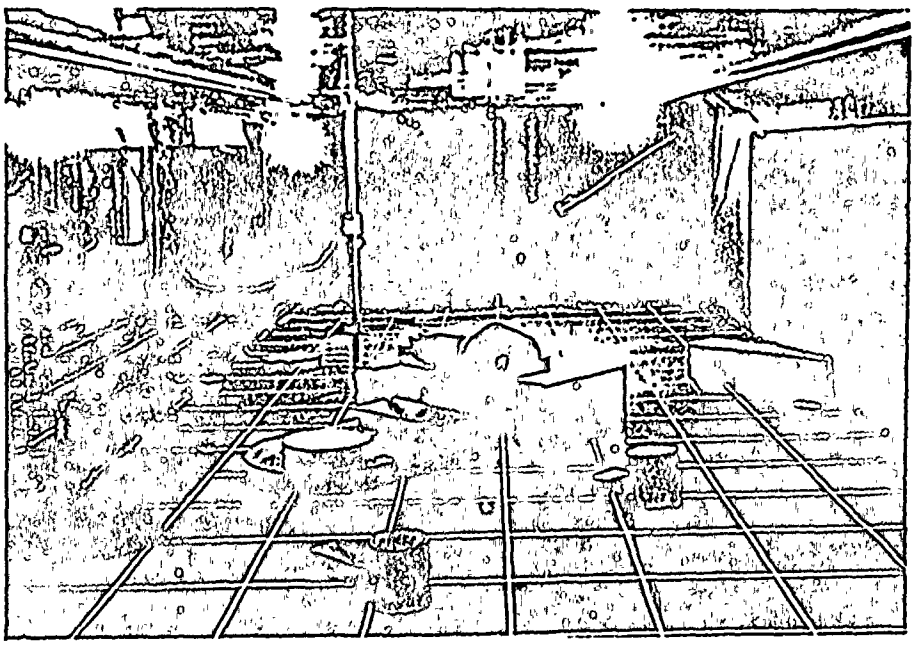

looking upwind

Fig. 2 Photographs of Model of NRTS Complex In the Wind Tunnel

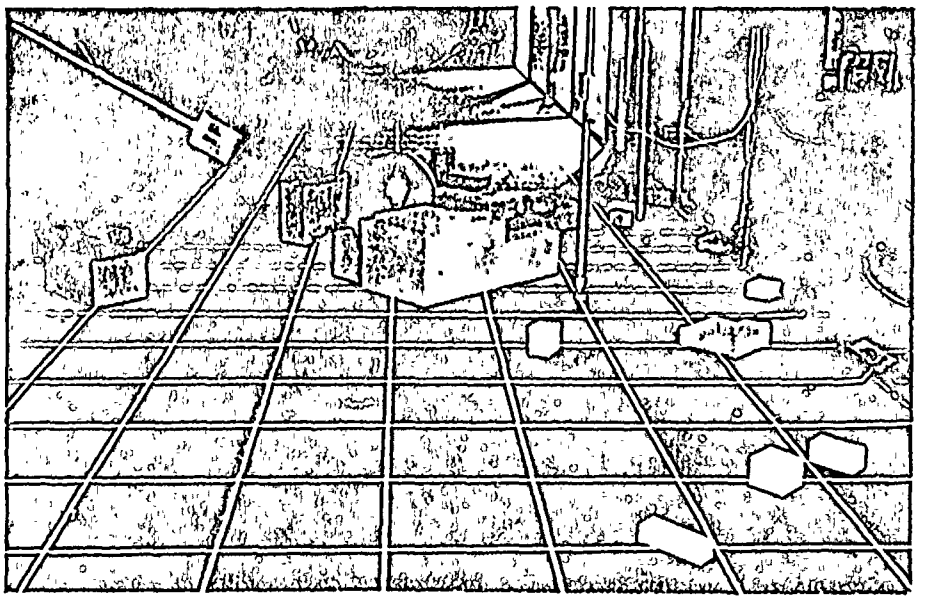

looking downwind

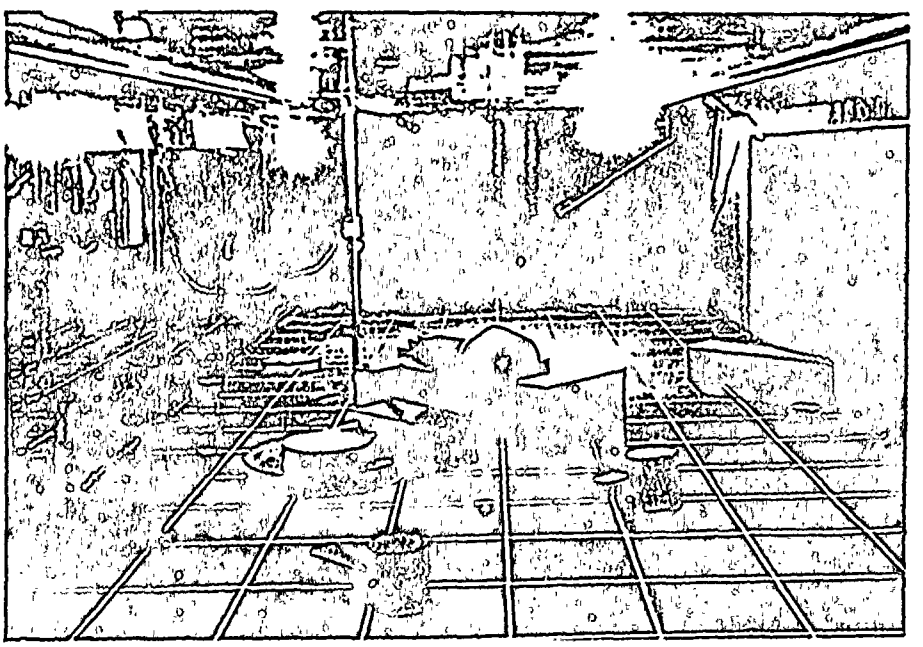

looking upwind

Fig. 2 Photographs of Model of NRTS Complex In the Wind Tunnel

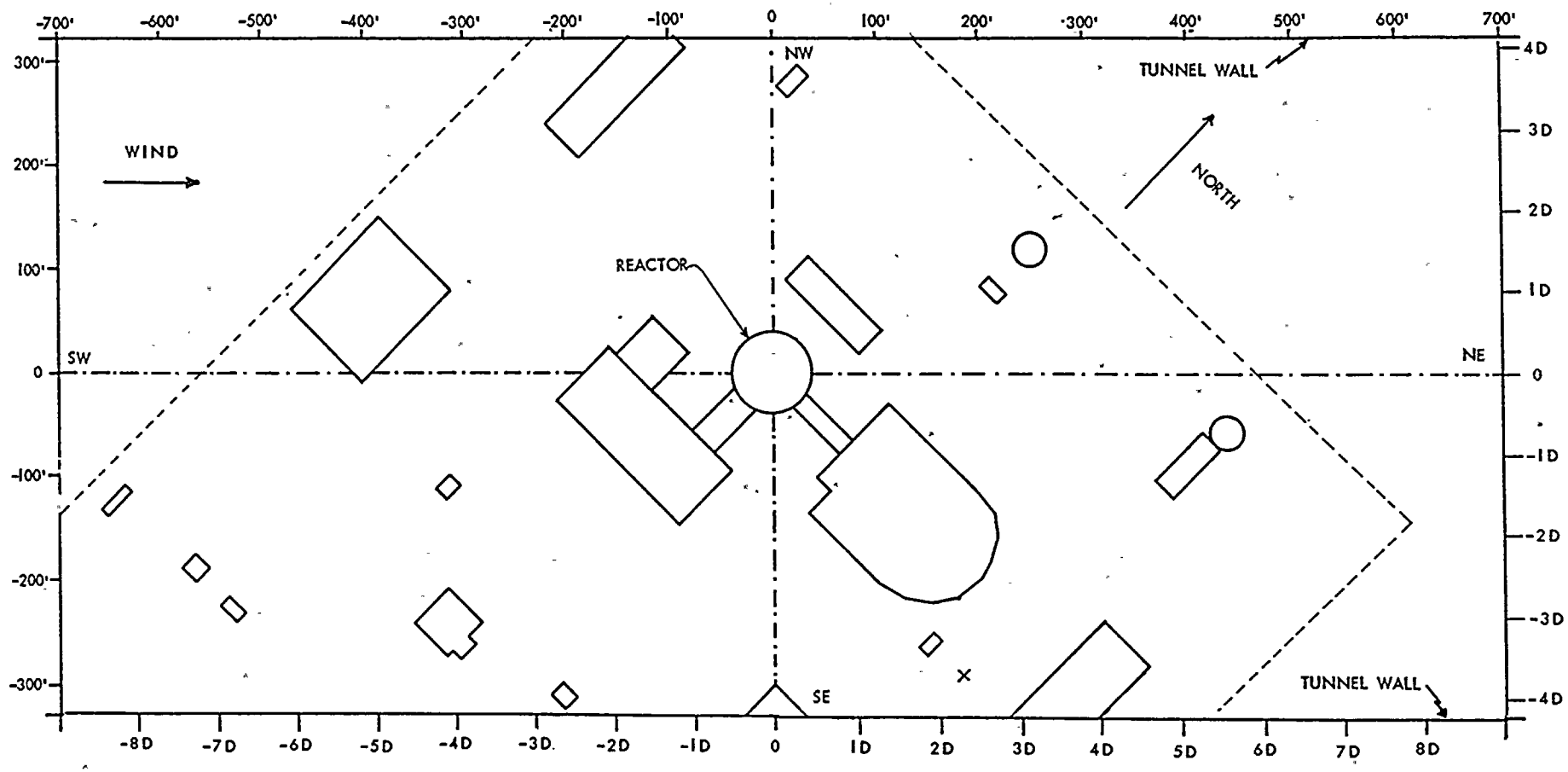

Fig. 3 Arrangement of NRTS Buildings in the Tunnel in a SW Wind

D = Reactor shell diameter = 80 ft.

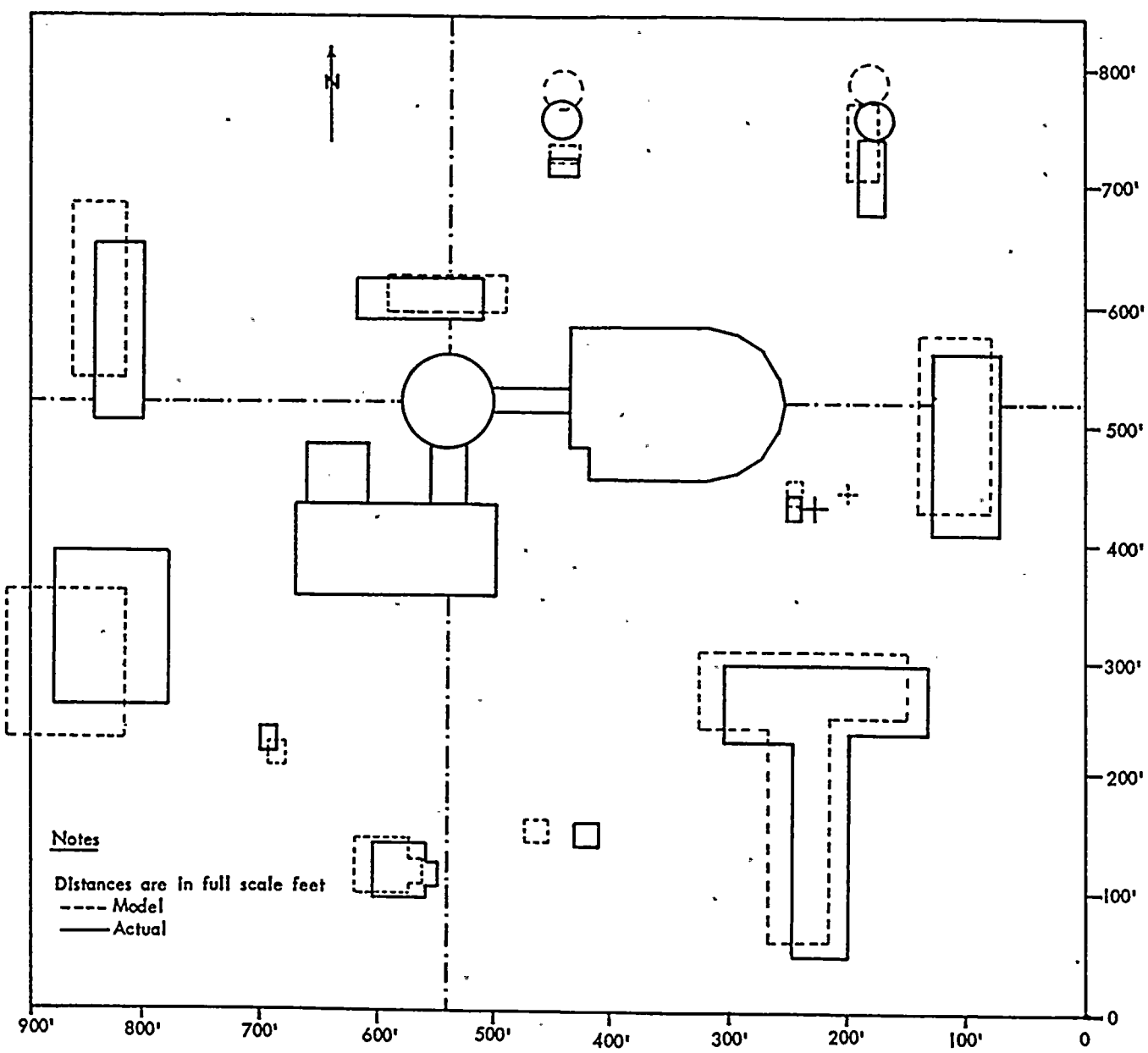

Fig. 4 Comparison of Model and Actual Building Arrangements at NRTS

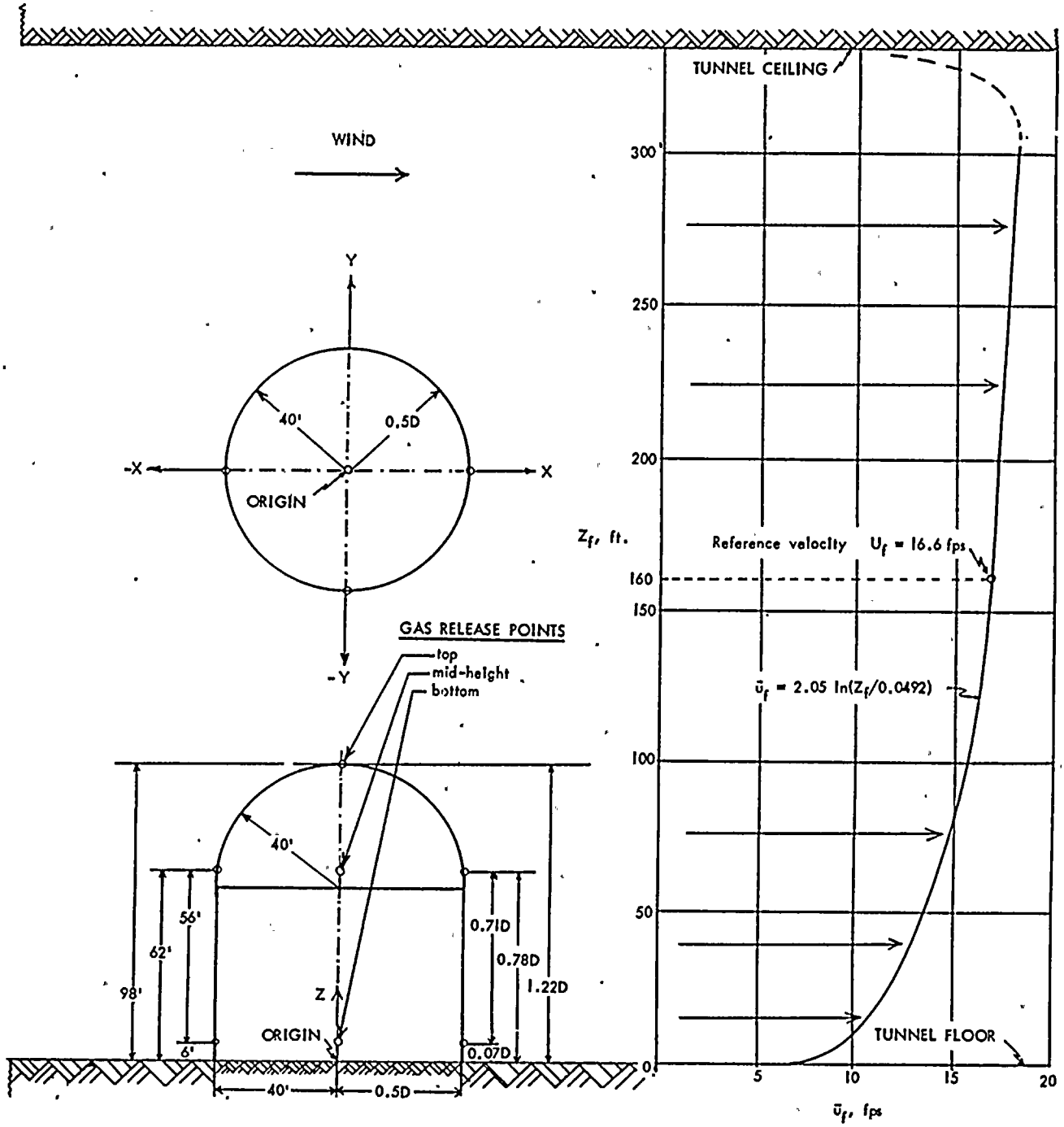

Fig. 5 EBR II Model Dimensions and Wind Velocity Profile

Dimensions are in equivalent full scale feet
D = Reactor shell diameter = 80 ft.

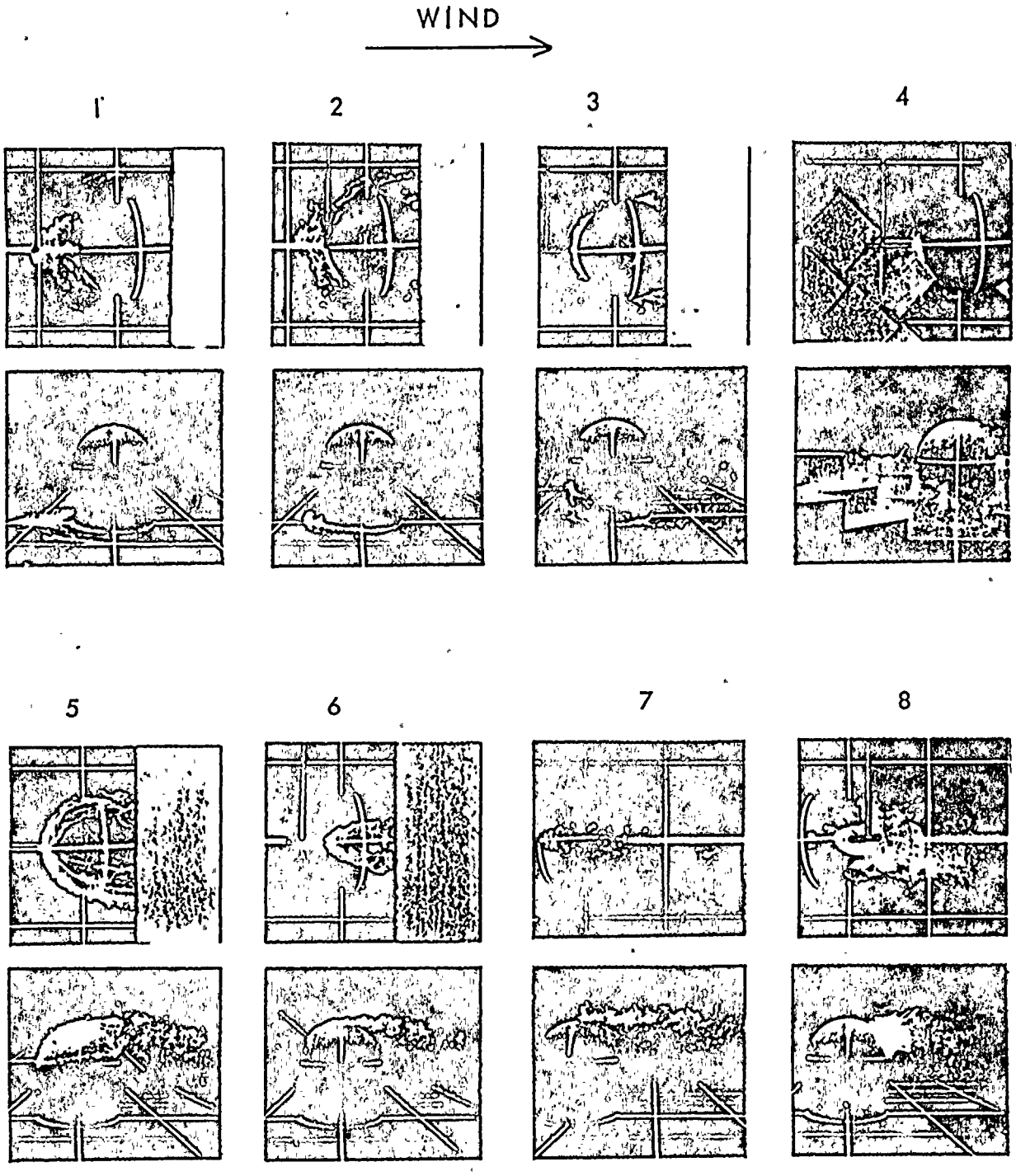

Fig. 6 Photographic Sequence Showing Diffusion of Smoke Released at Various Points In the Longitudinal Centerplane through the Reactor Shell

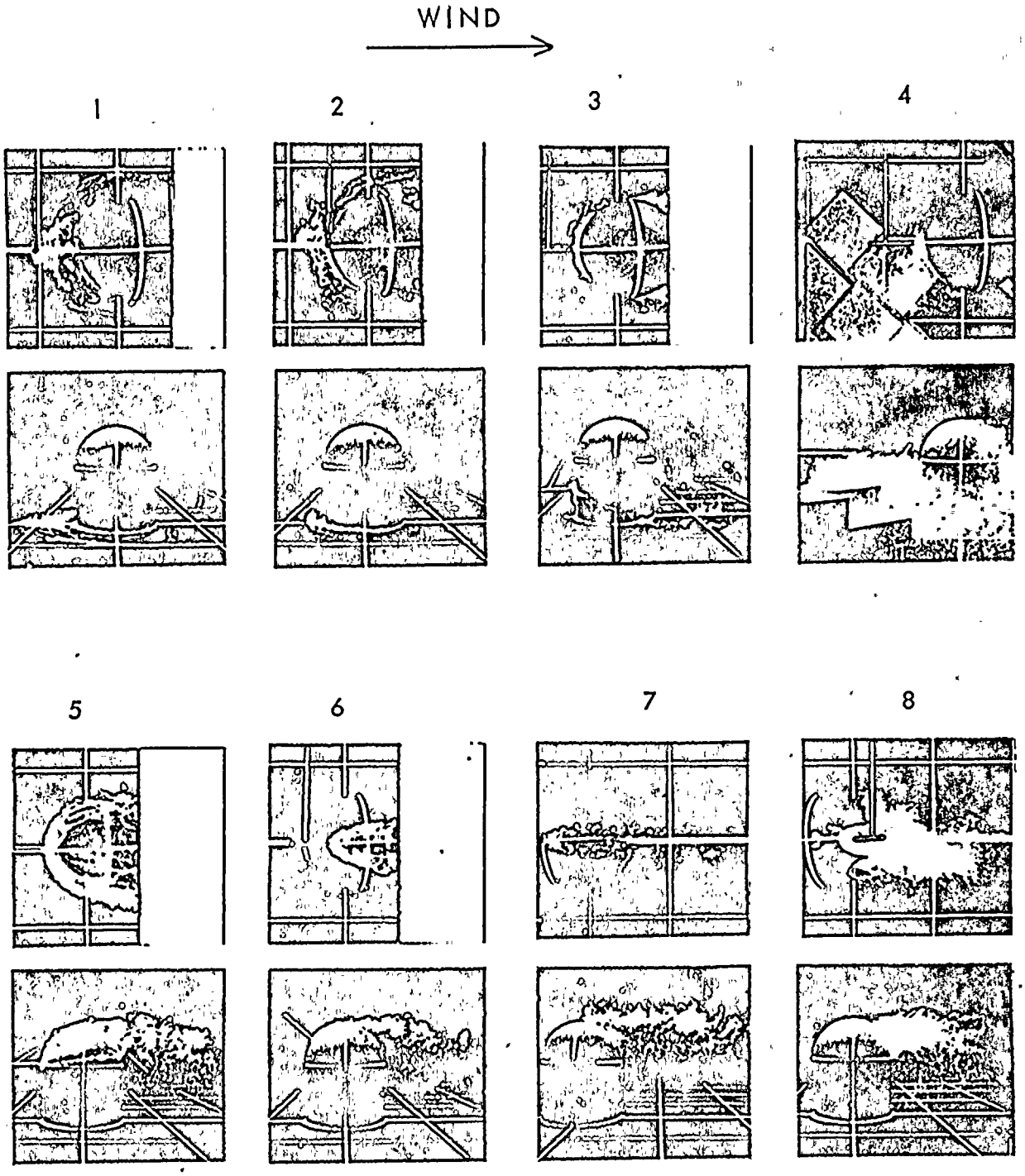

Fig. 6 Photographic Sequence Showing Diffusion of Smoke Released at Various Points In the Longitudinal Centerplane through the Reactor Shell

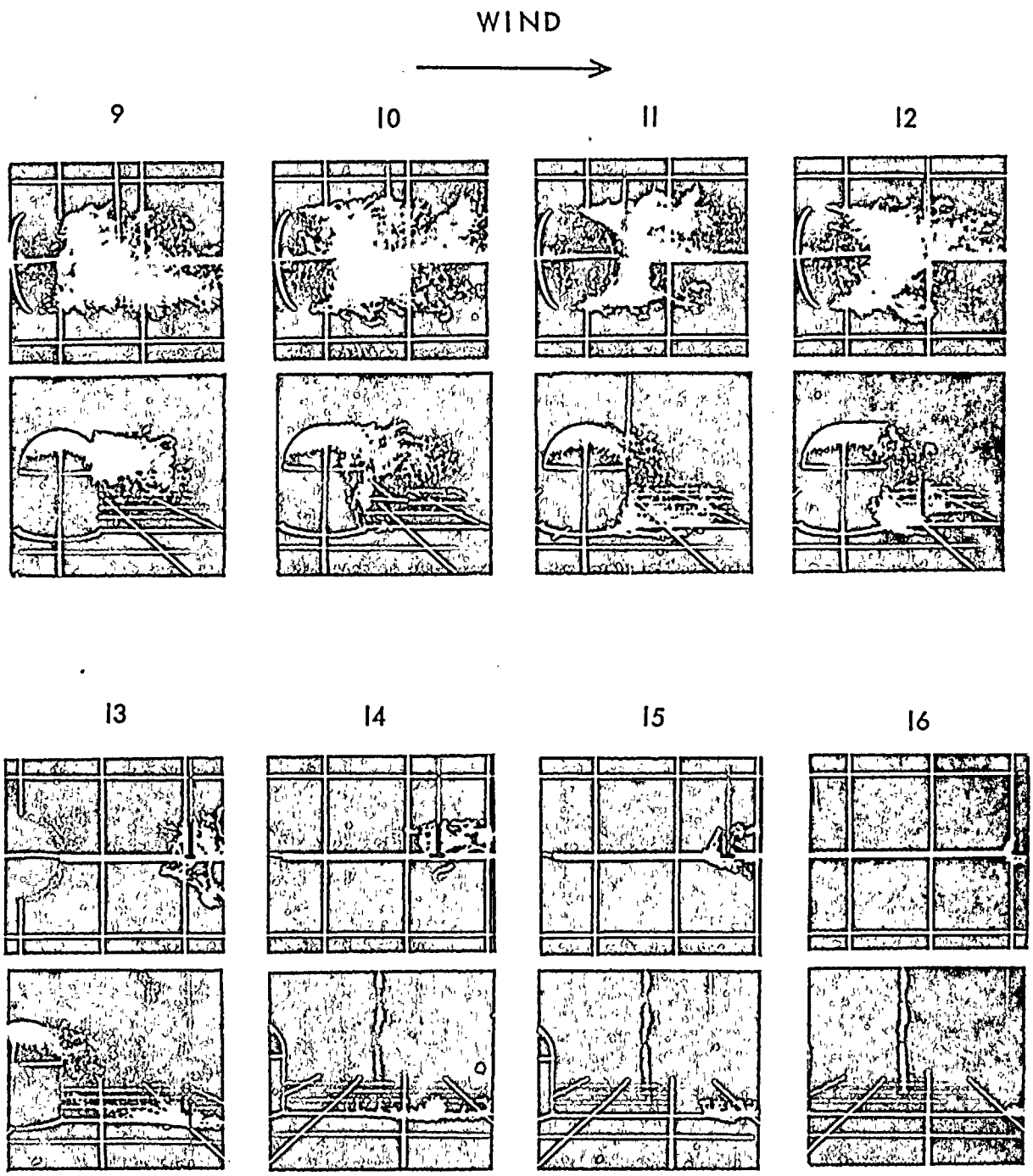

Fig. 6 (cont.) Photographic Sequence Showing Diffusion of Smoke Released at Various Points in the Longitudinal Centerplane through the Reactor Shell

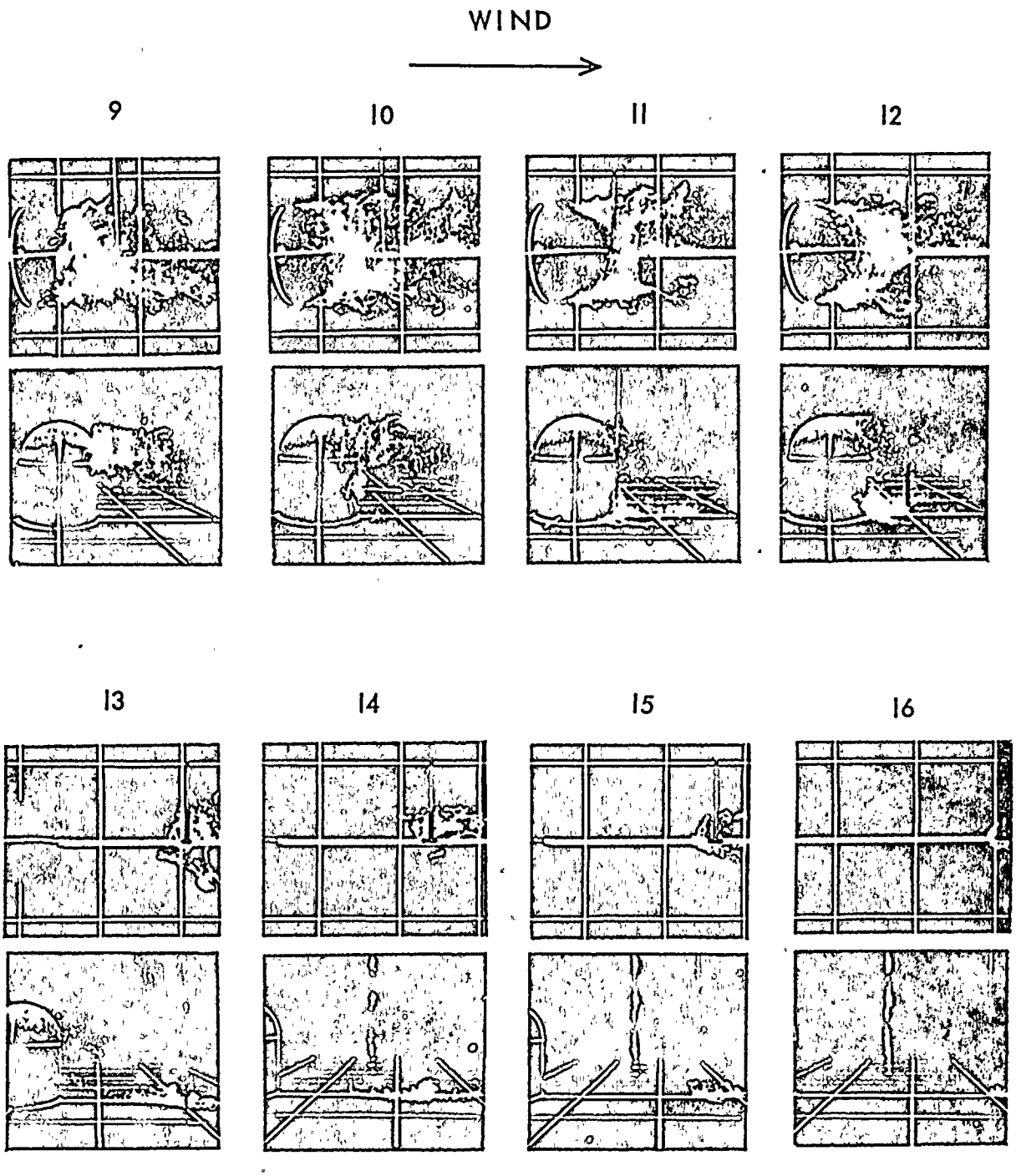

Fig. 6 (cont.) Photographic Sequence Showing Diffusion of Smoke Released at Various Points in the Longitudinal Centerplane through the Reactor Shell

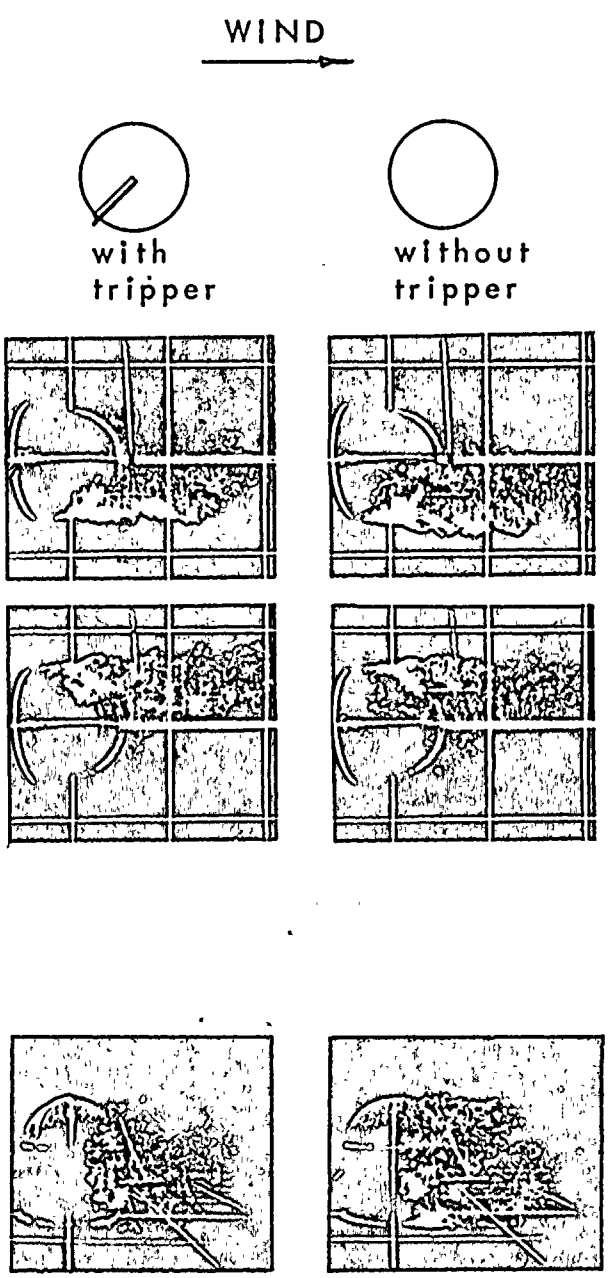

Fig. 7 Photographs of Smoke Diffusion Downwind of Reactor Shell With and Without Boundary Layer Control

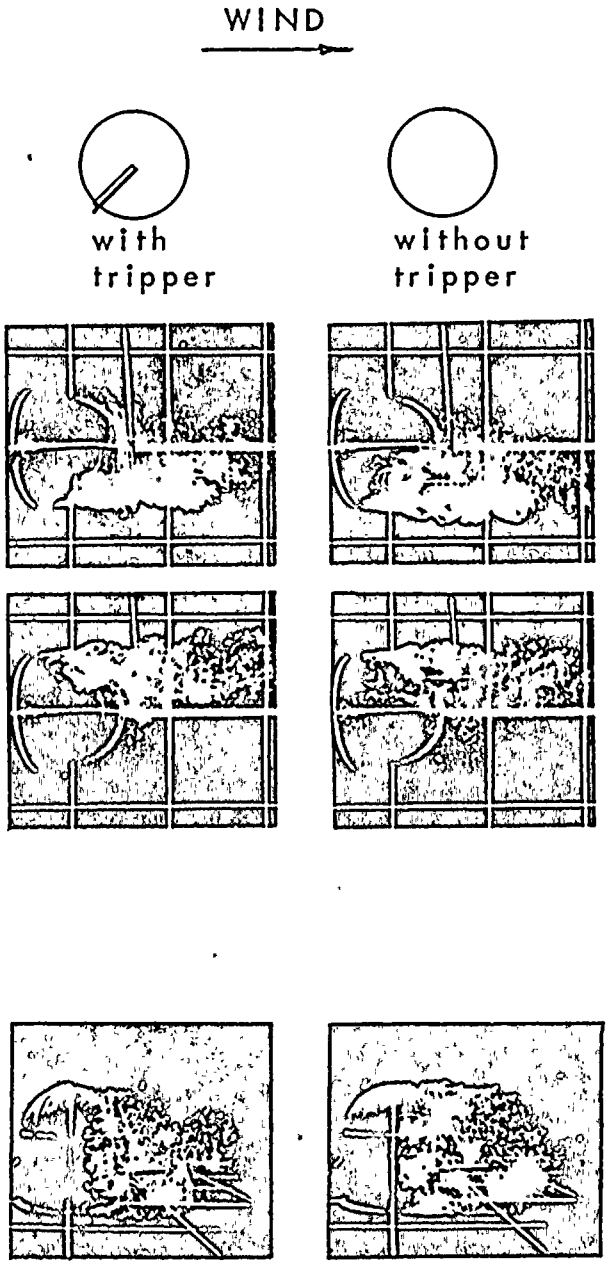

Fig. 7 Photographs of Smoke Diffusion Downwind of Reactor Shell With and Without Boundary Layer Control

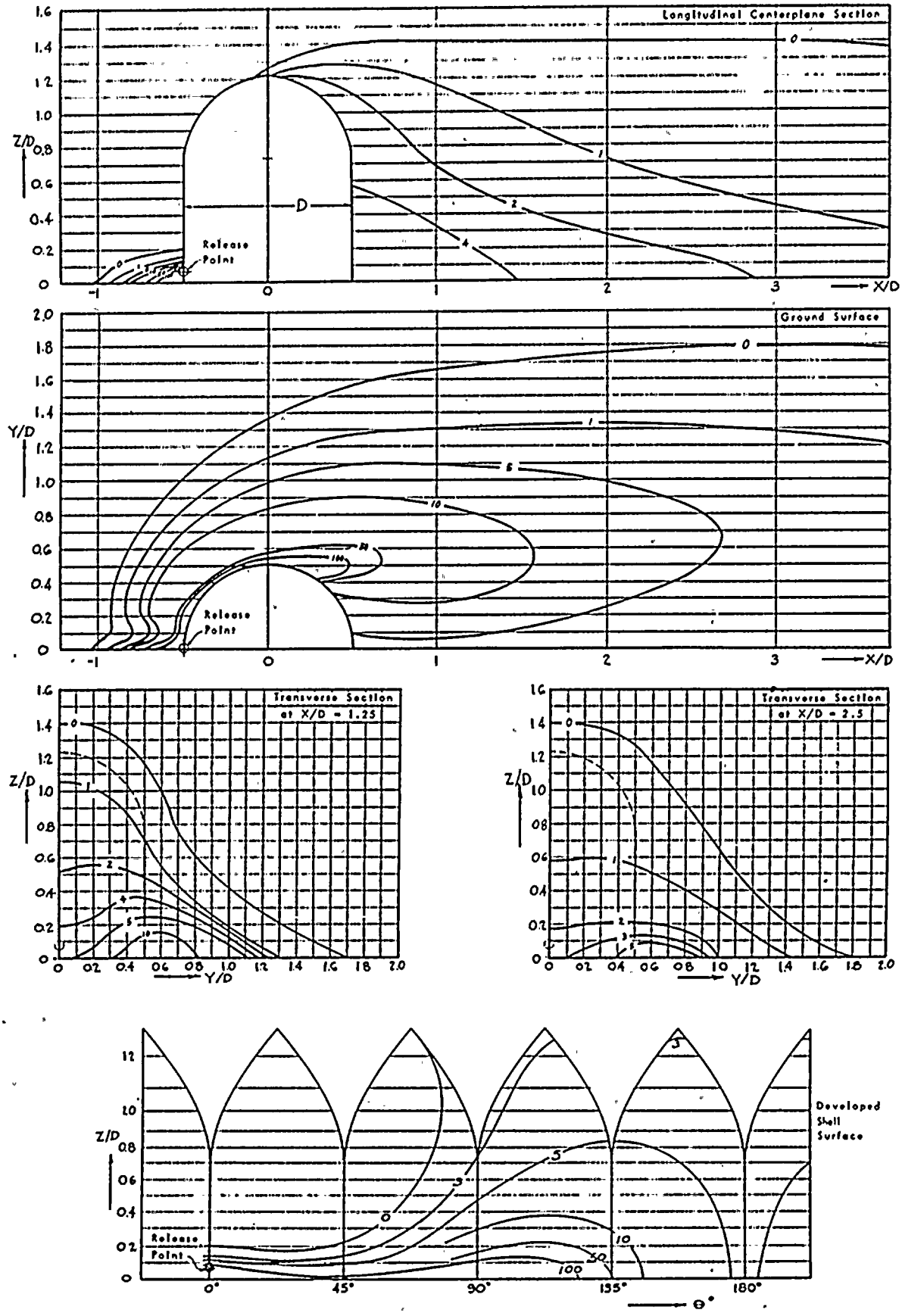

Fig. 8 K – Isopleths for Gas Released through Reactor Shell

Configuration:	shell alone
Release point:	bottom upwind
Wind :	log profile, 5.54 fps

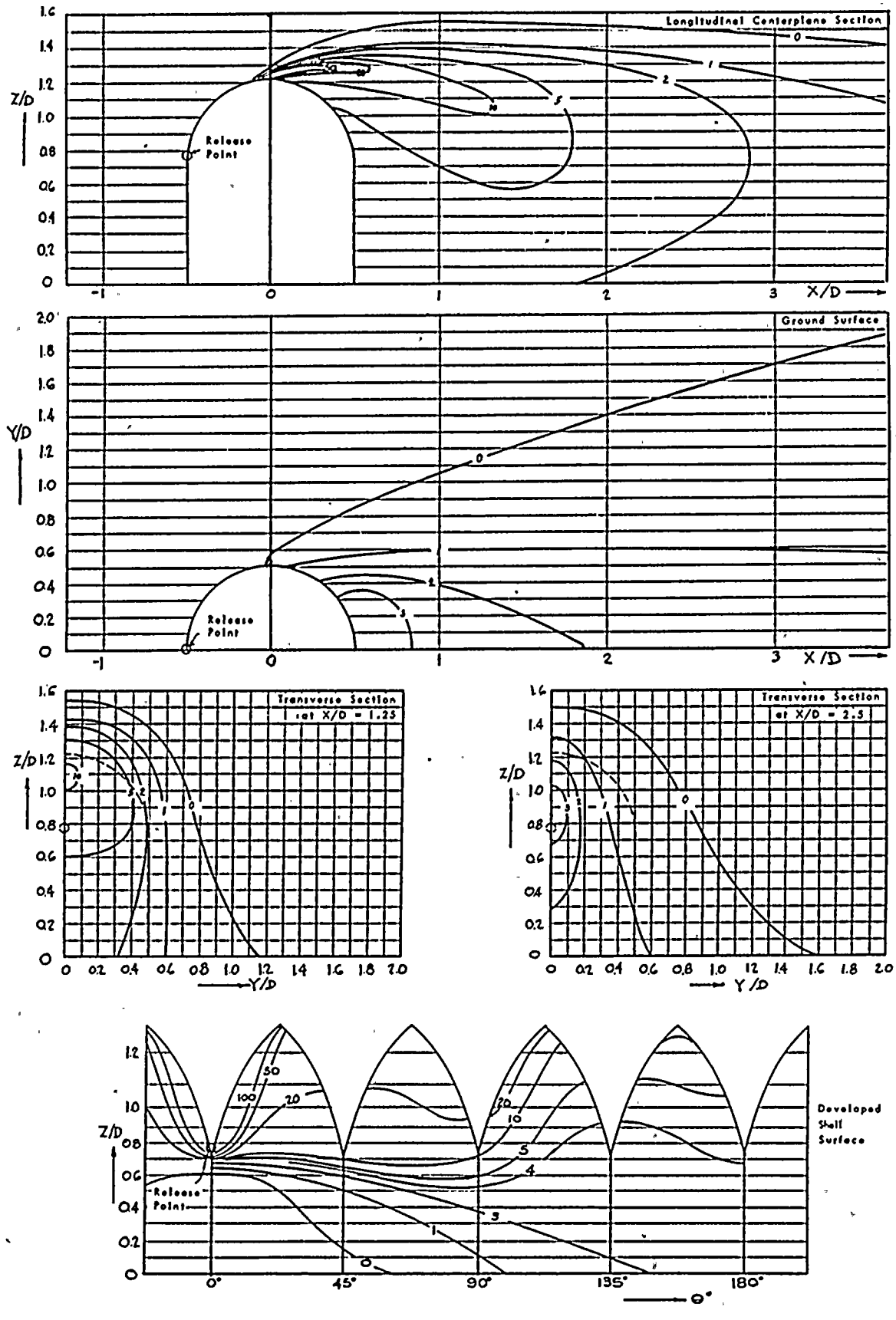

Fig. 9 K - Isopleths for Gas Released through Reactor Shell

Configuration : shell alone
Release point : mid-height upwind
Wind : log profile, 5.56 fps

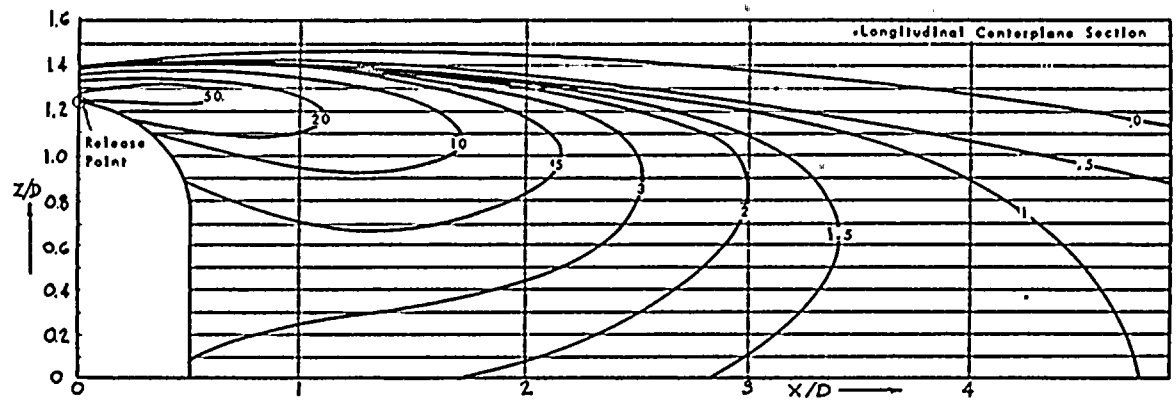

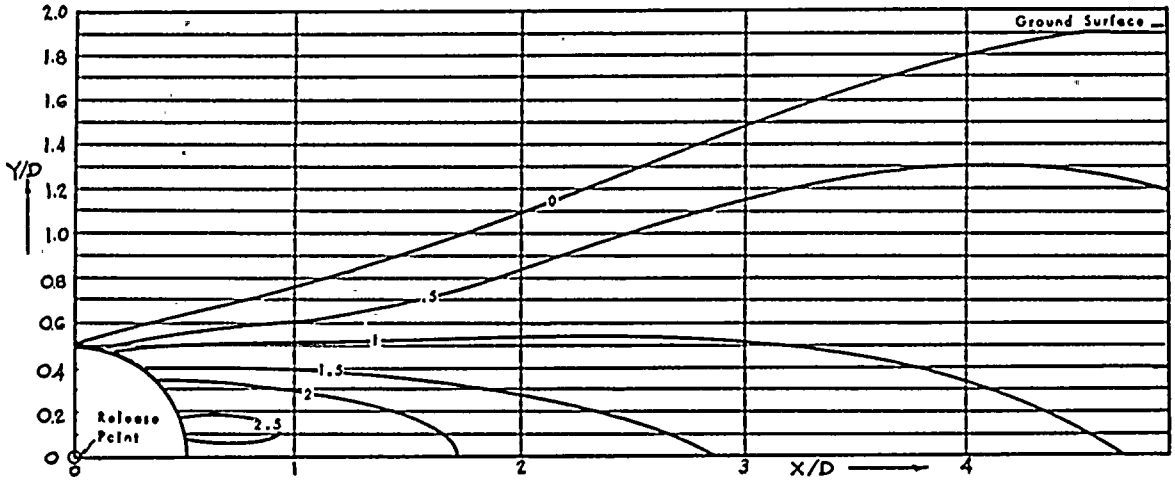

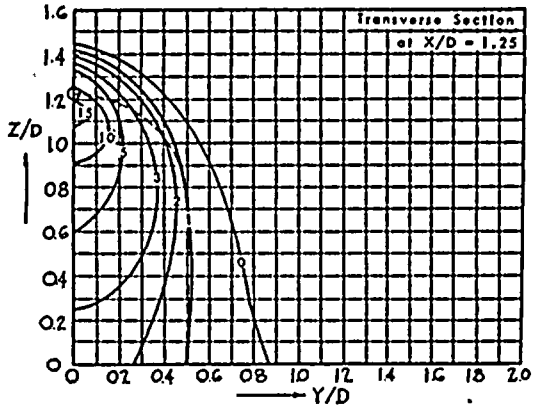

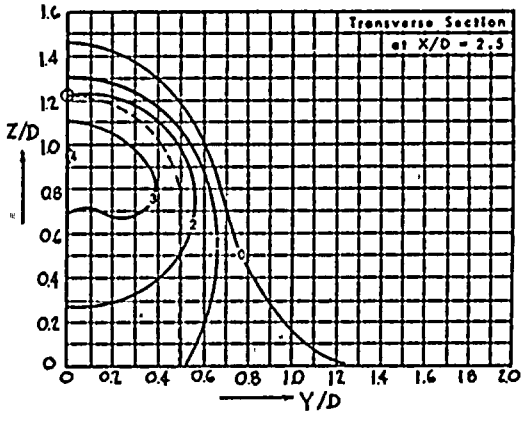

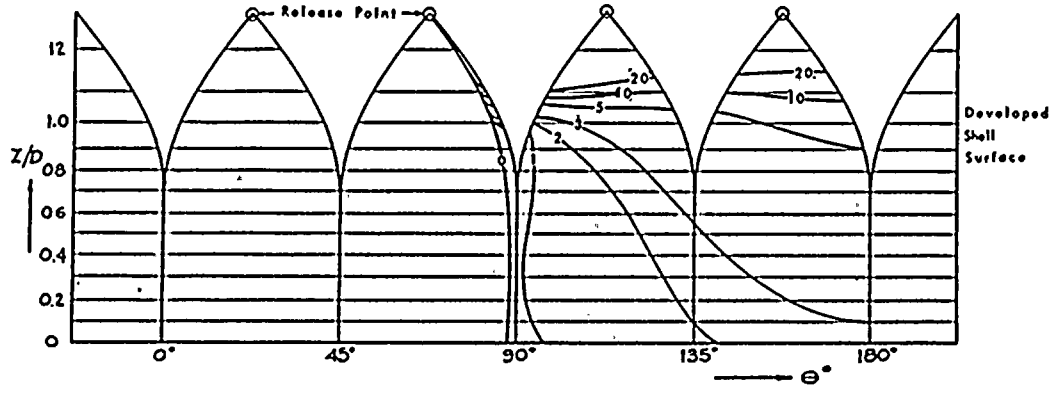

Fig. 10 K,- Isopleths for Gas Released through Reactor Shell

Configuration : shell alone
Release point : top
Wind : log profile, 5.54 fps

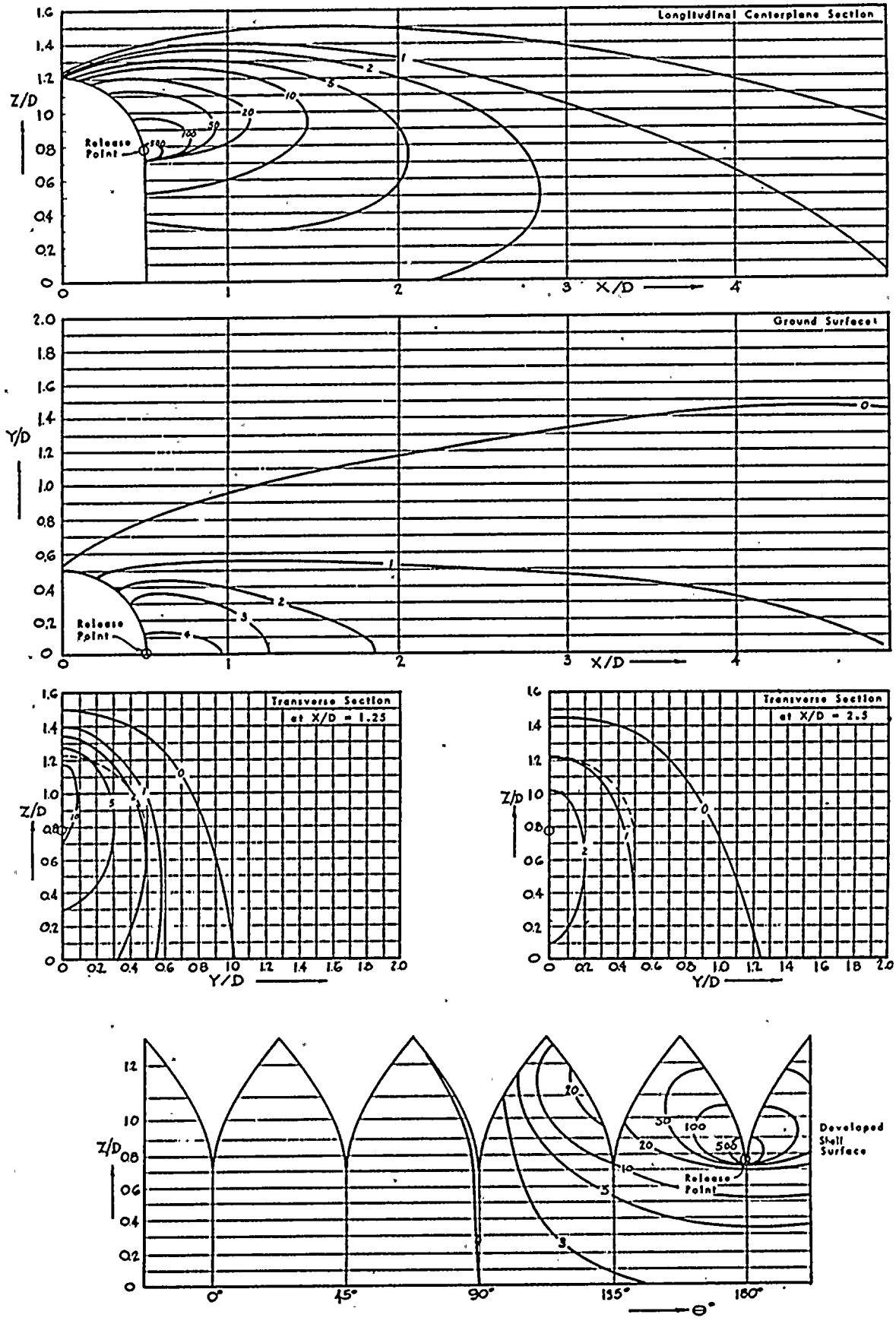

Fig. 11 K – Isopleths for Gas Released through Reactor Shell

Configuration : shell alone
Release point : mid-height downwind
Wind : log profile, 5.54 fps

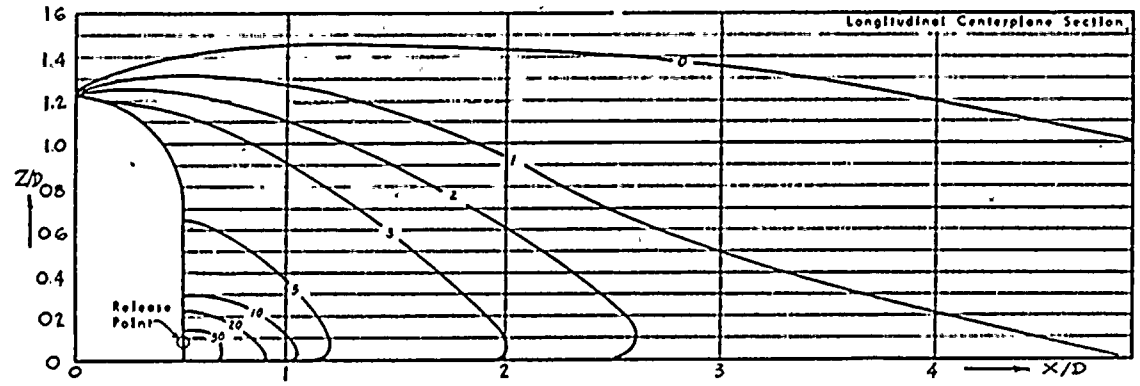

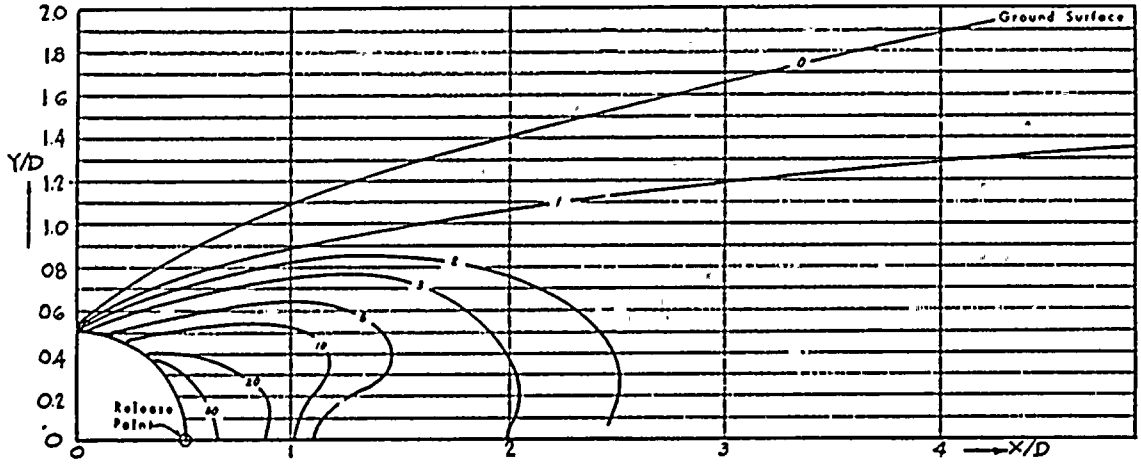

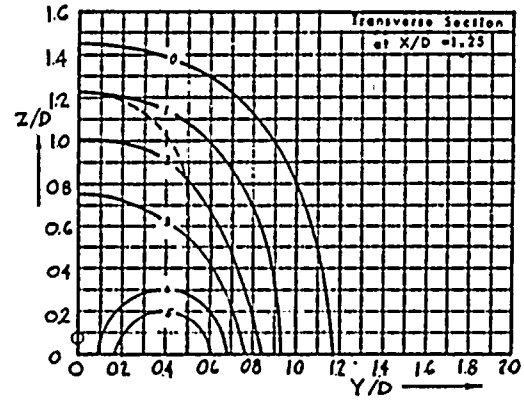

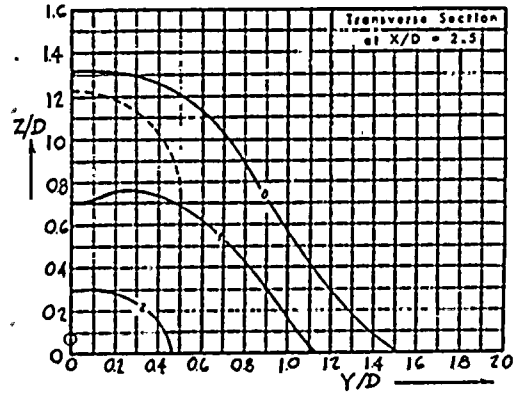

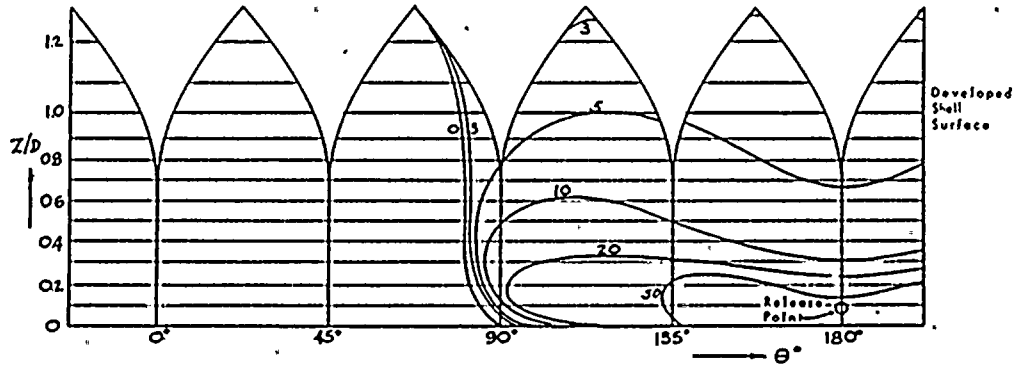

Fig. 12 K = Isopleths for Gas Released through Reactor Shell

Configuration :	shell alone
Release point :	bottom downwind
Wind " :	log profile, 5.54 fps

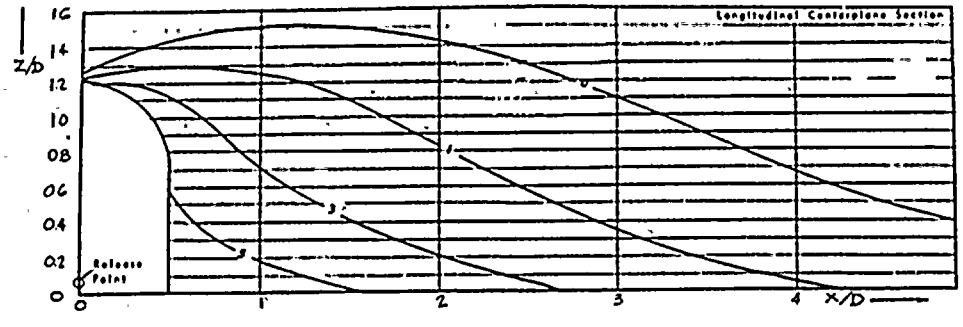

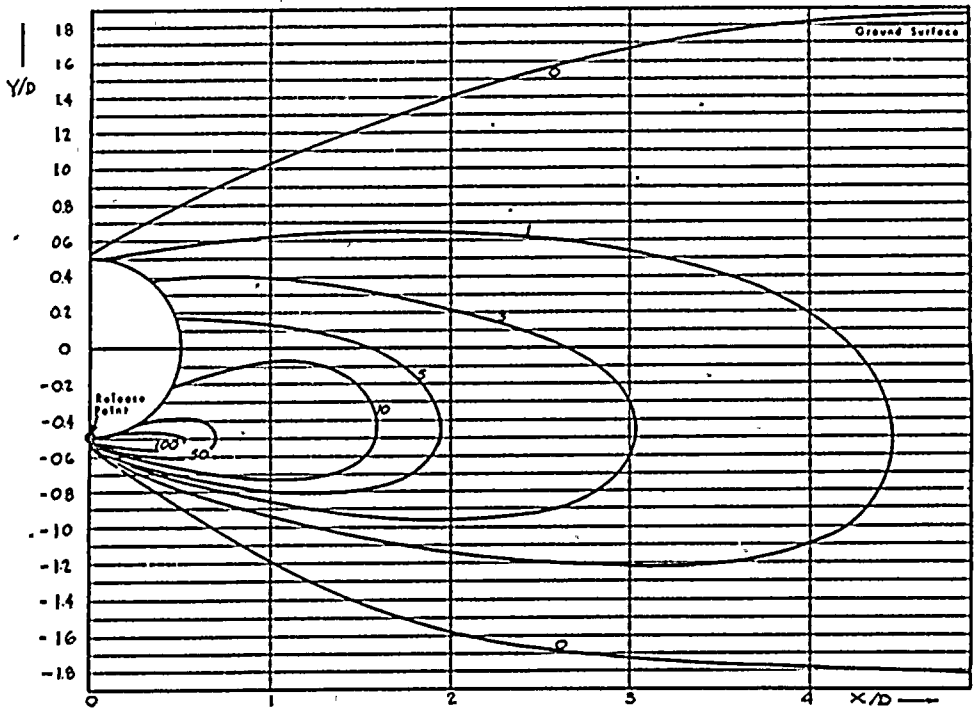

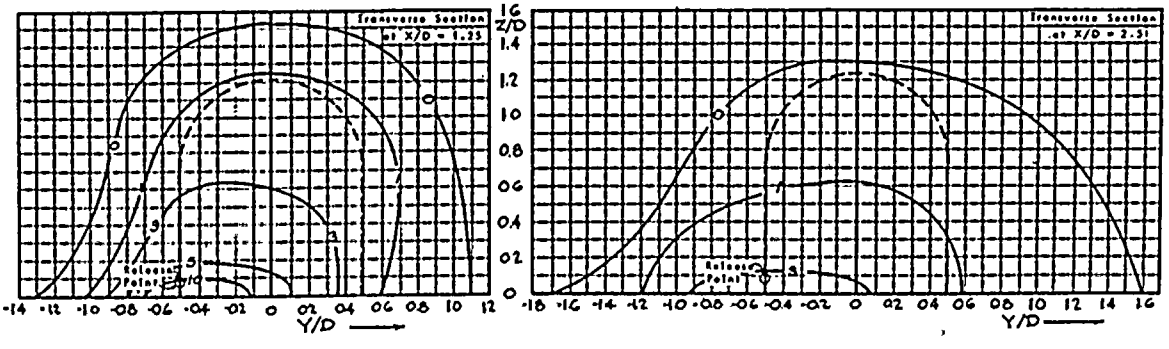

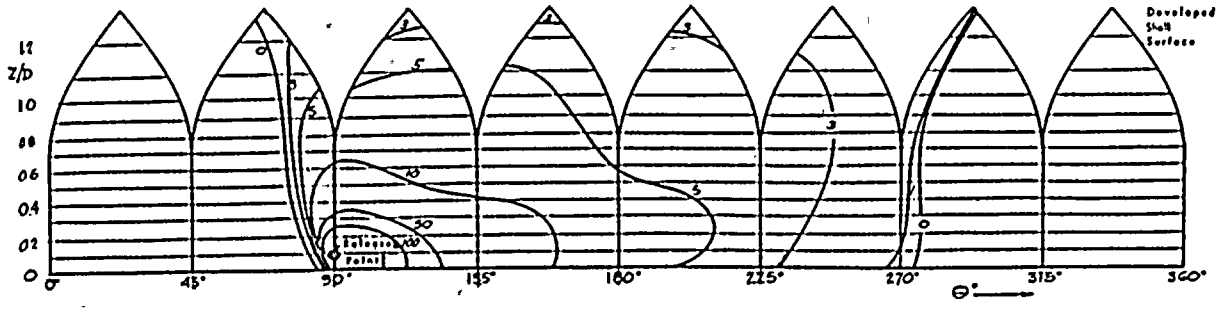

Fig. 13 K-Isopleths for Gas Released through Scooter Shell

Configuration: shell alone
Release point: bottom slot
Wind: log profile, 5.34 f/s

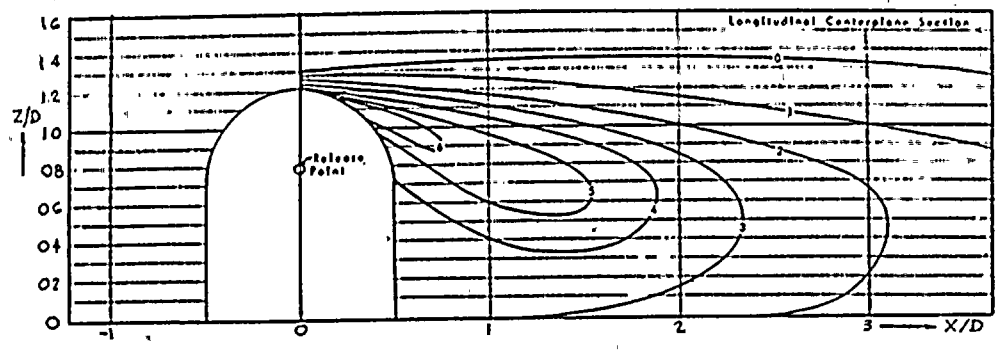

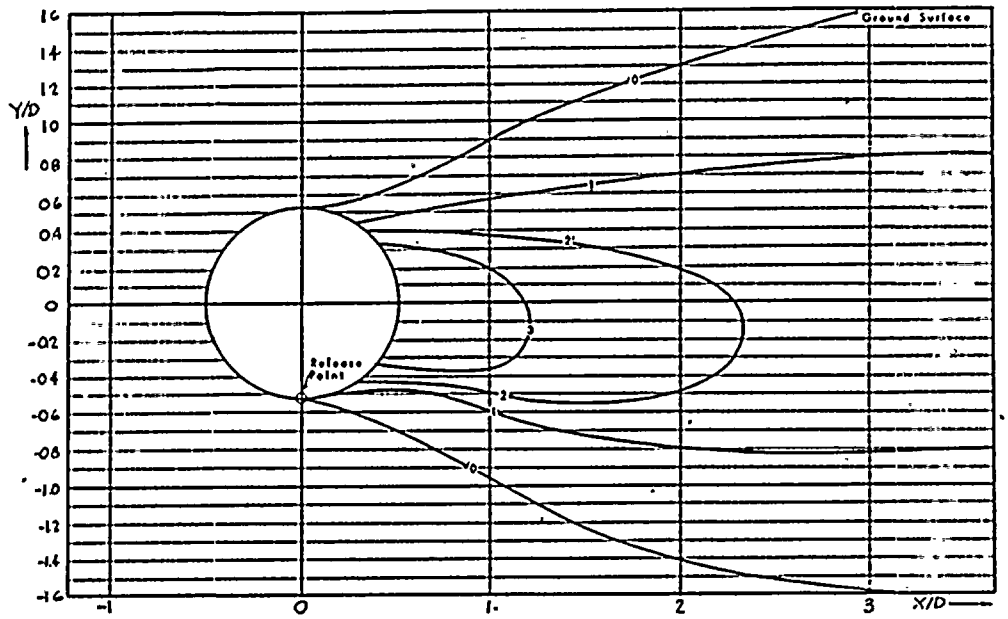

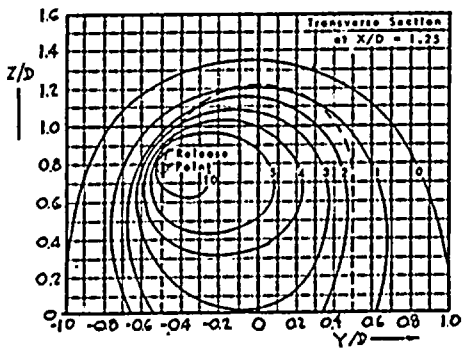

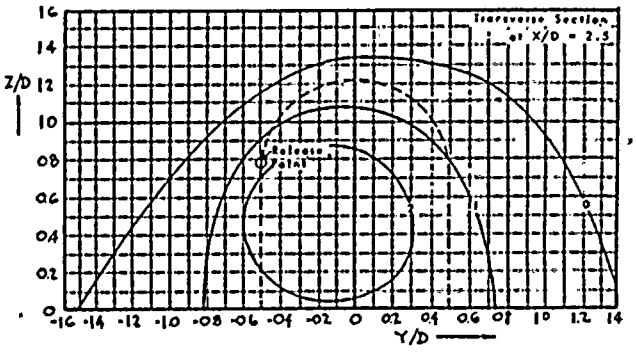

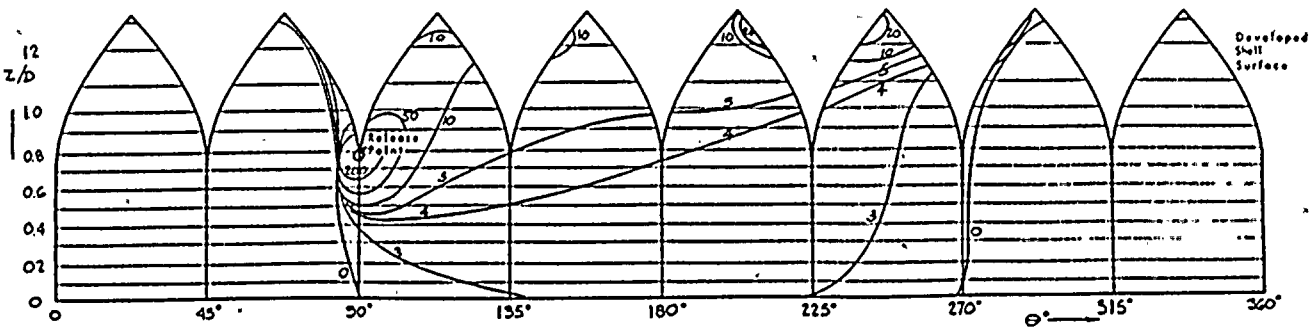

Fig. 14 K-Isoplets for Gas Released through Reactor Shell

Configuration : shell alone
Release point : mid-height side
Wind : log profile, 5.54 fps

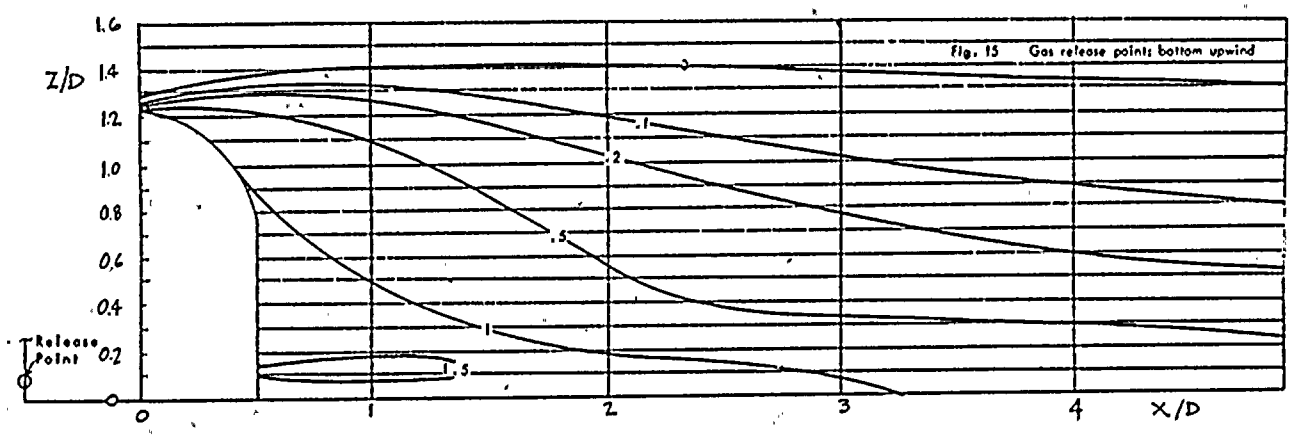

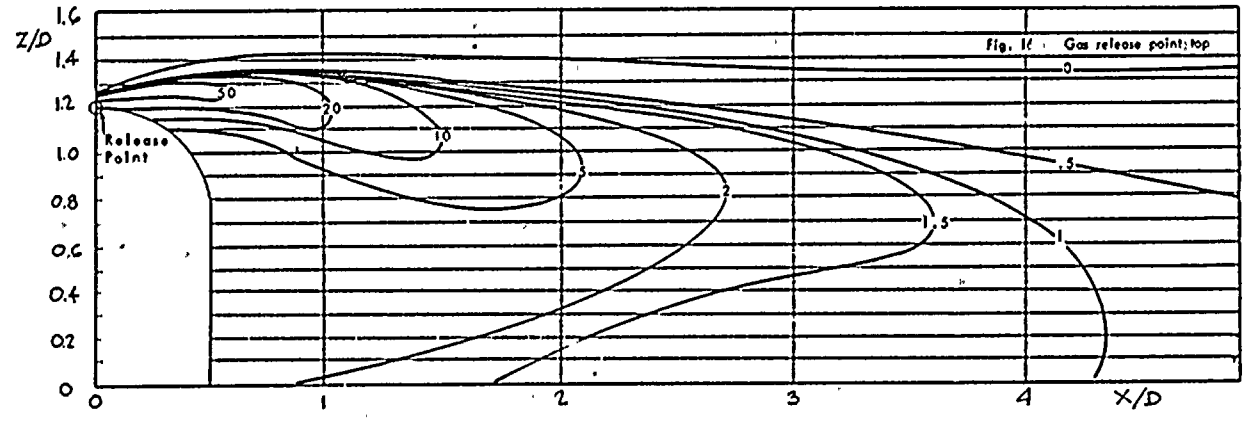

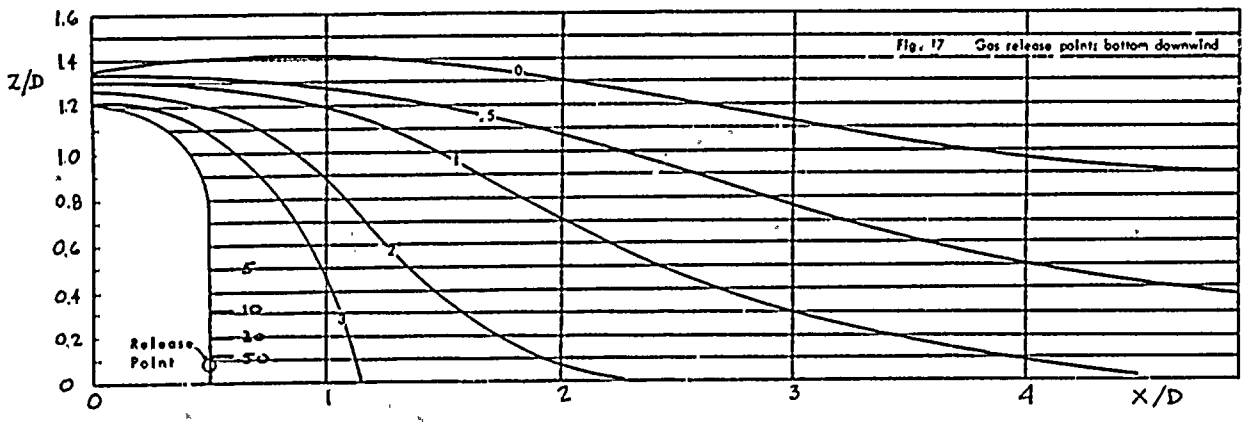

Figs. 15 to 17 . K - Isopleths for Gas Released through Reactor Shell

Configuration	:	shell alone
Release point	:	variable
Wind	:	uniform profile, 5.54 fps
Surveys	:	longitudinal centerplane

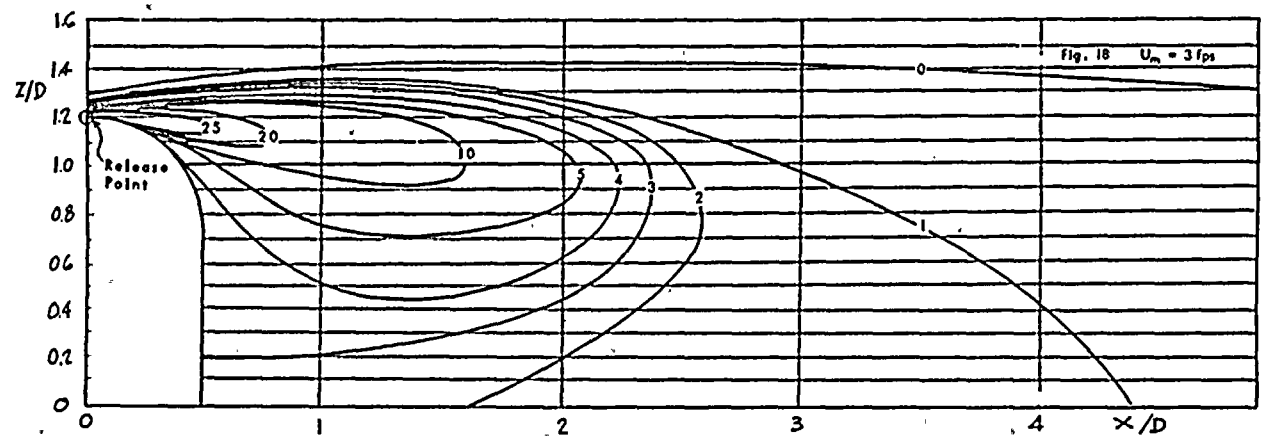

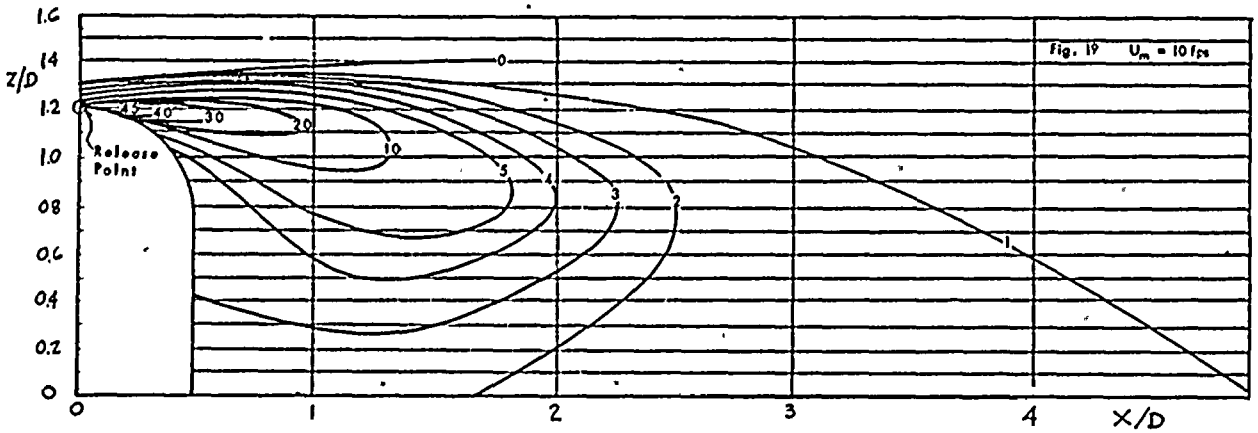

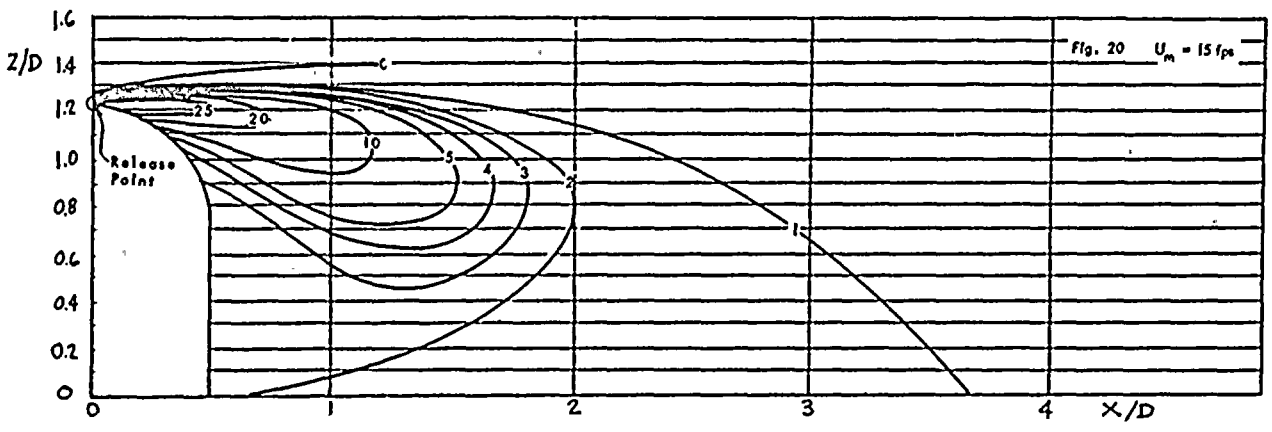

Figs. 18 to 20 K – Isopleths for Gas Released through Reactor Shell

Configuration	:	shell alone
Release point	:	top
Wind	:	uniform profile, 3, 10, and 15 fps
Surveys	:	longitudinal centerplane

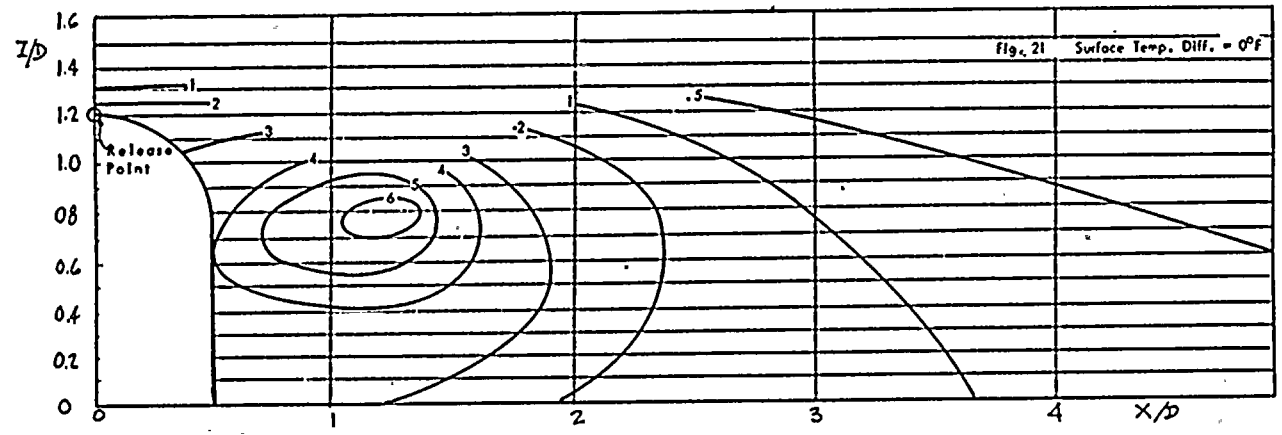

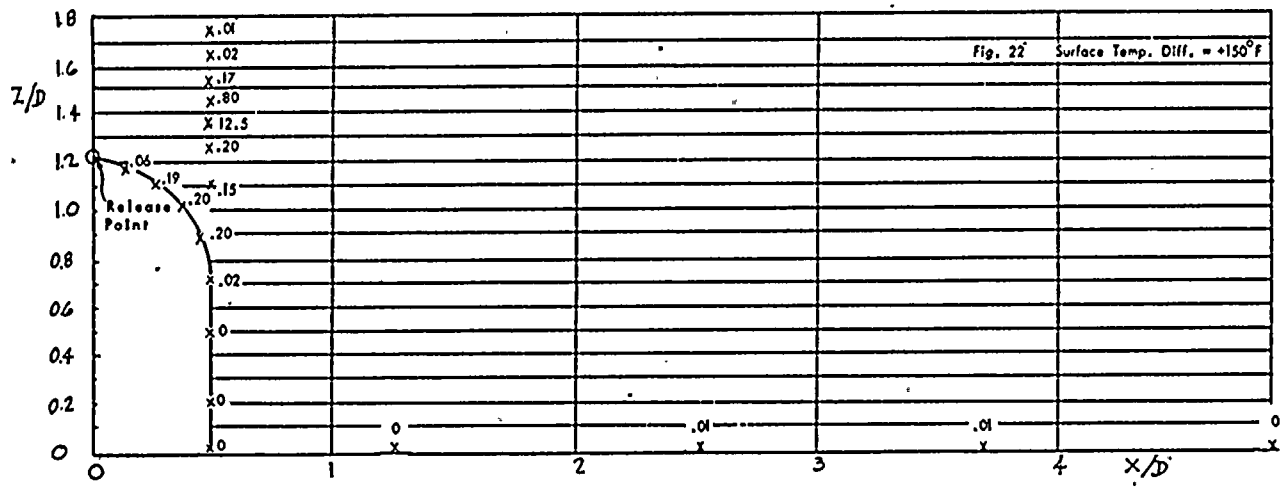

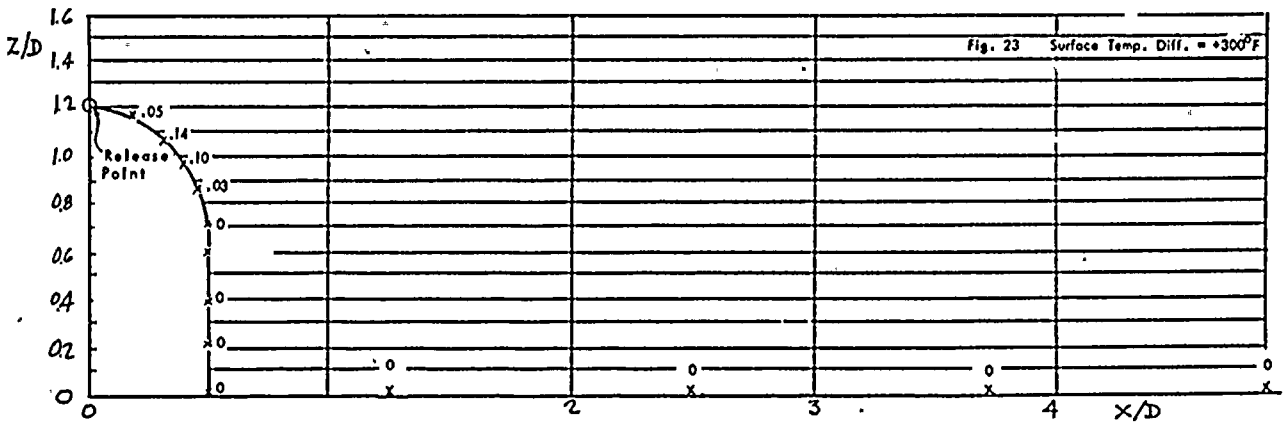

Figs. 21 to 23 K – Isopleths for Gas Released through Reactor Shell

Configuration	:	shell alone
Release point	:	top
Wind	:	log profile, 1.7 fps
Surf. temp. diff.	:	+0°F, +150°F, +300°F
Surveys	:	longitudinal centerplane

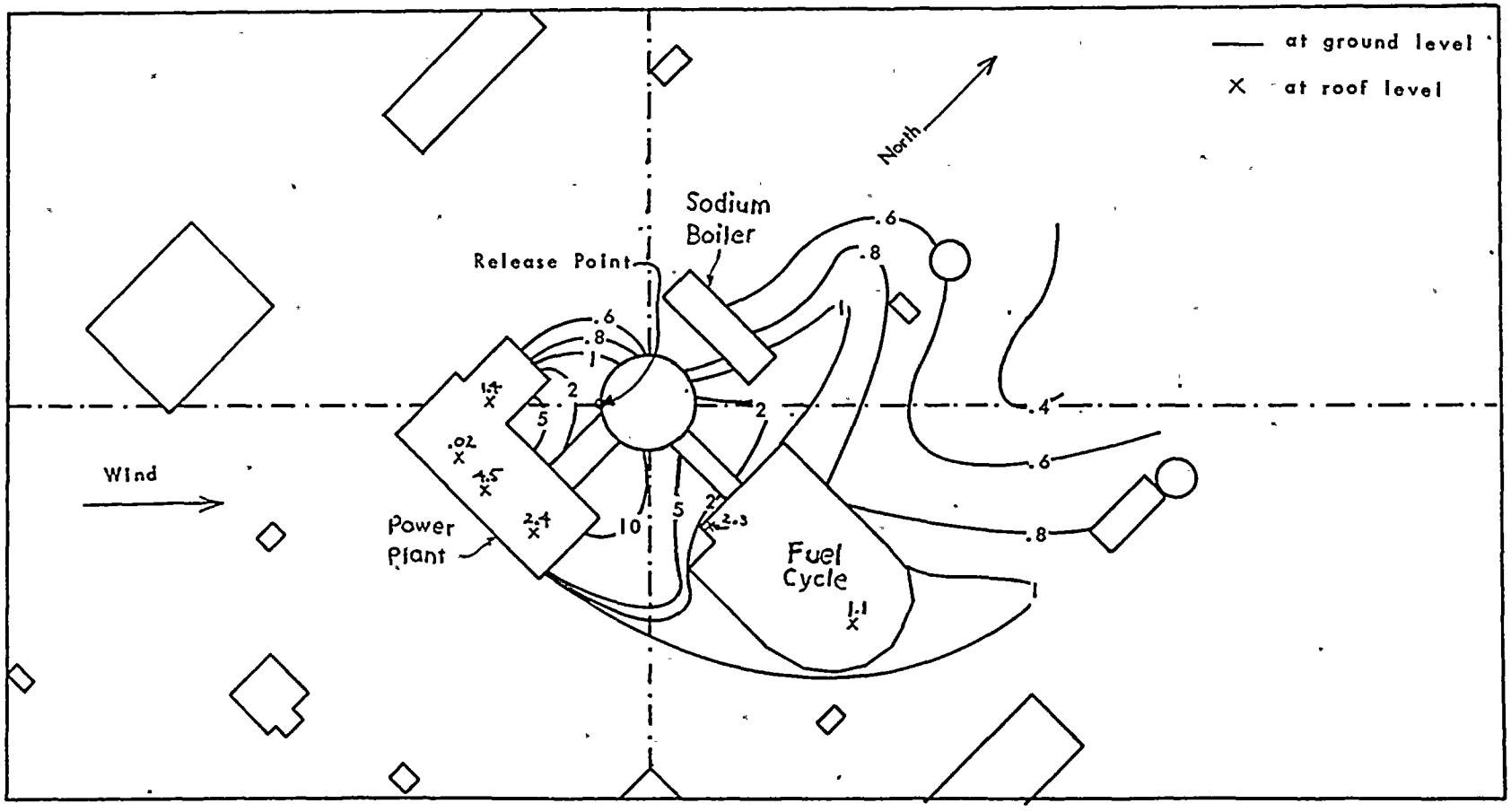

Fig. 24 K – Isopleths for Gas Released through Reactor Shell

Configuration : entire complex
Release point : bottom upwind
Wind : SW, log profile, 5.54 fps

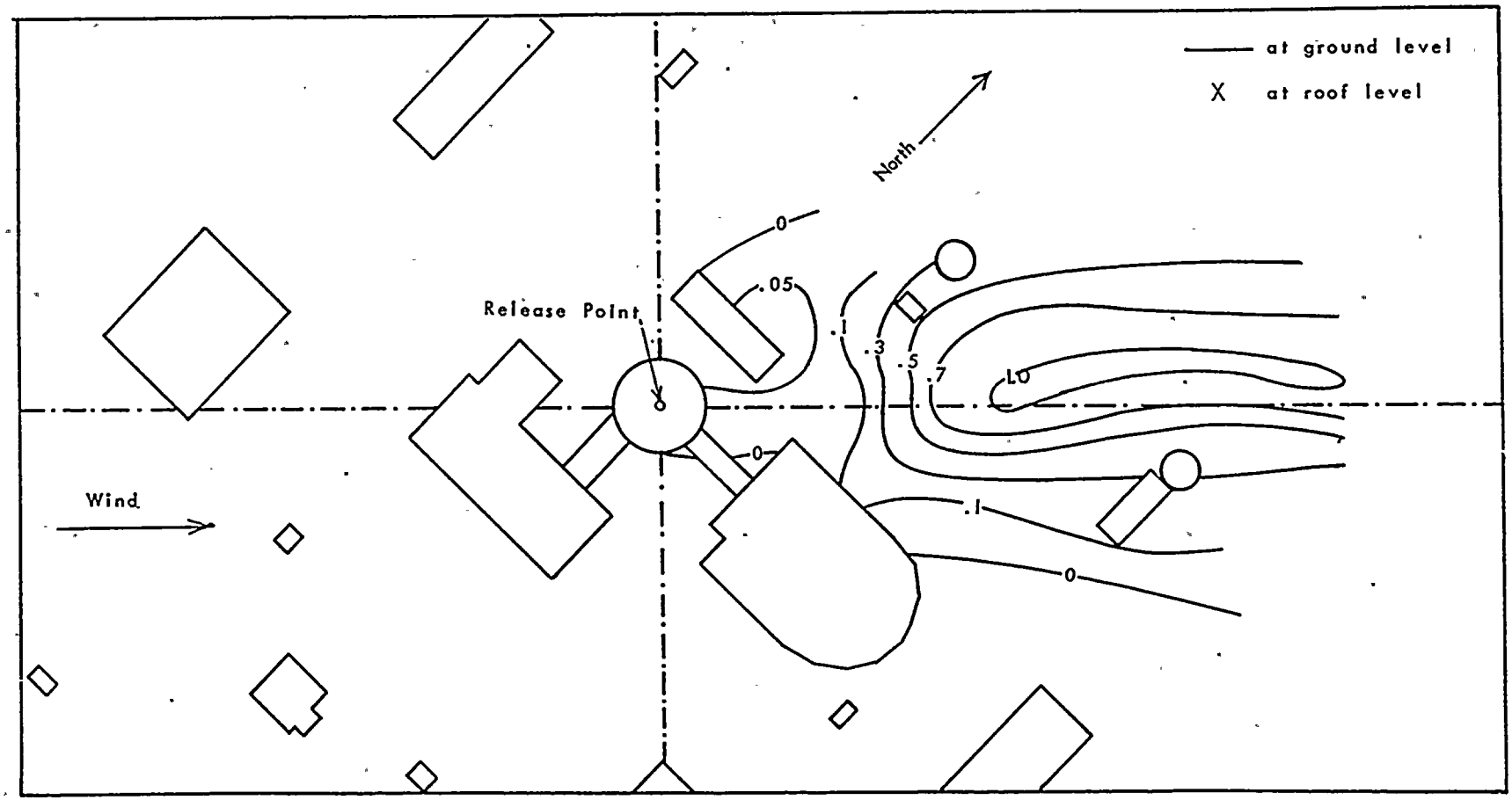

Fig. 25 K - Isopleths for Gas Released through Reactor Shell

Configuration : entire complex
Release point : top
Wind : SW, log profile, 5.54 fps

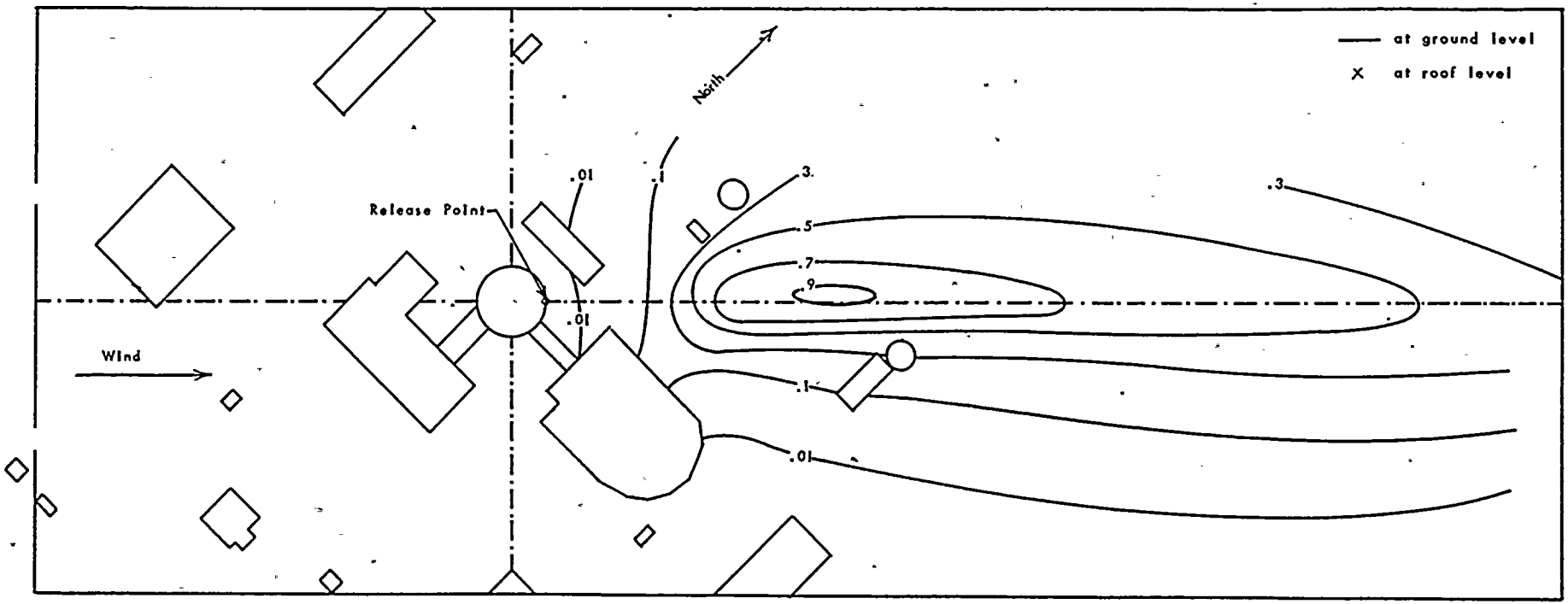

Fig. 26 K – Isopleths for Gas Released through Reactor Shell

Configuration : entire complex
Release point : mid-height downwind
Wind : SW, log profile, 5.54 fps

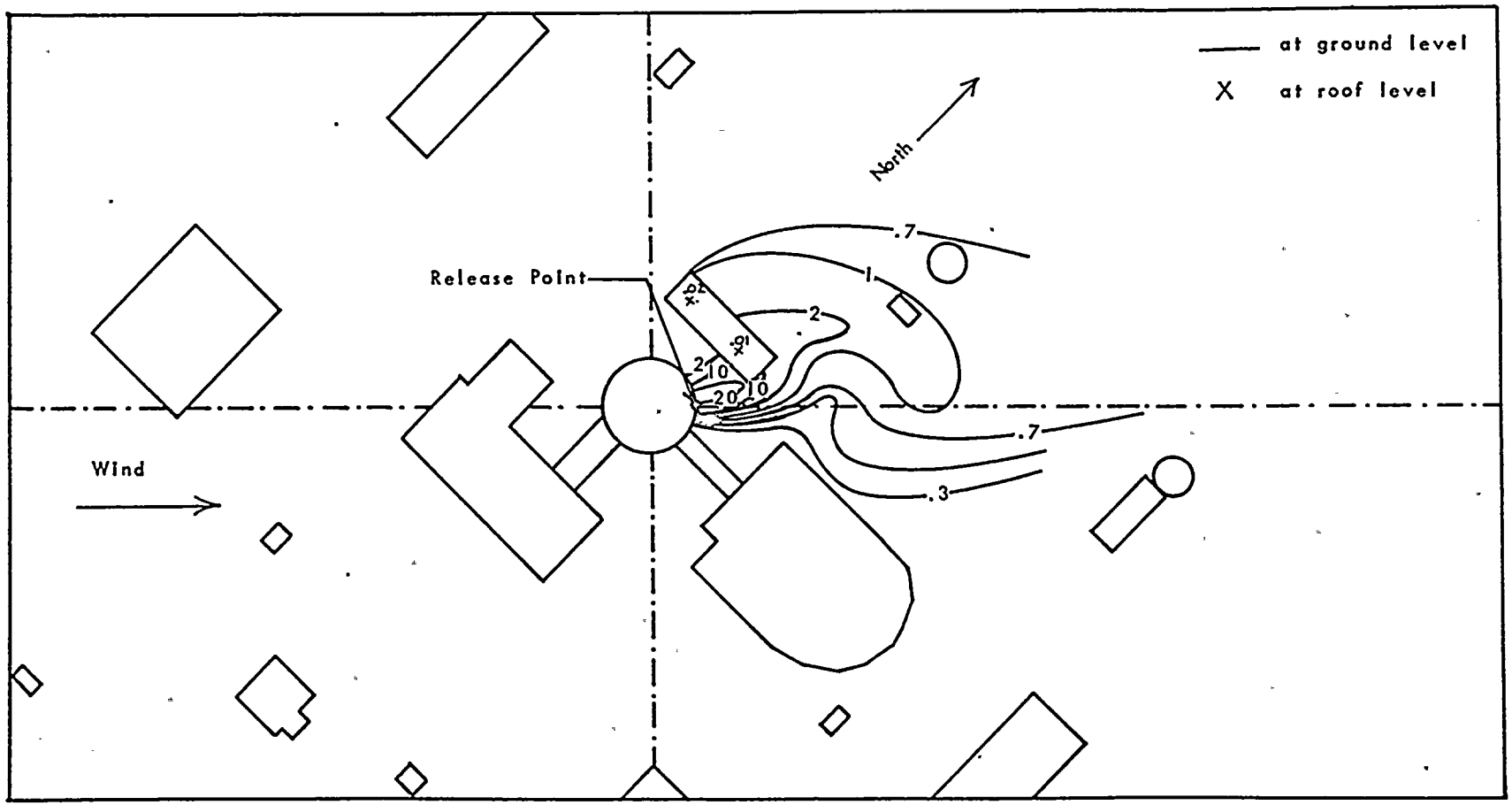

Fig. 27 K - Isopleths for Gas Released through Reactor Shell

Configuration : entire complex
Release point : bottom downwind
Wind : SW, log profile, 5.54 fps

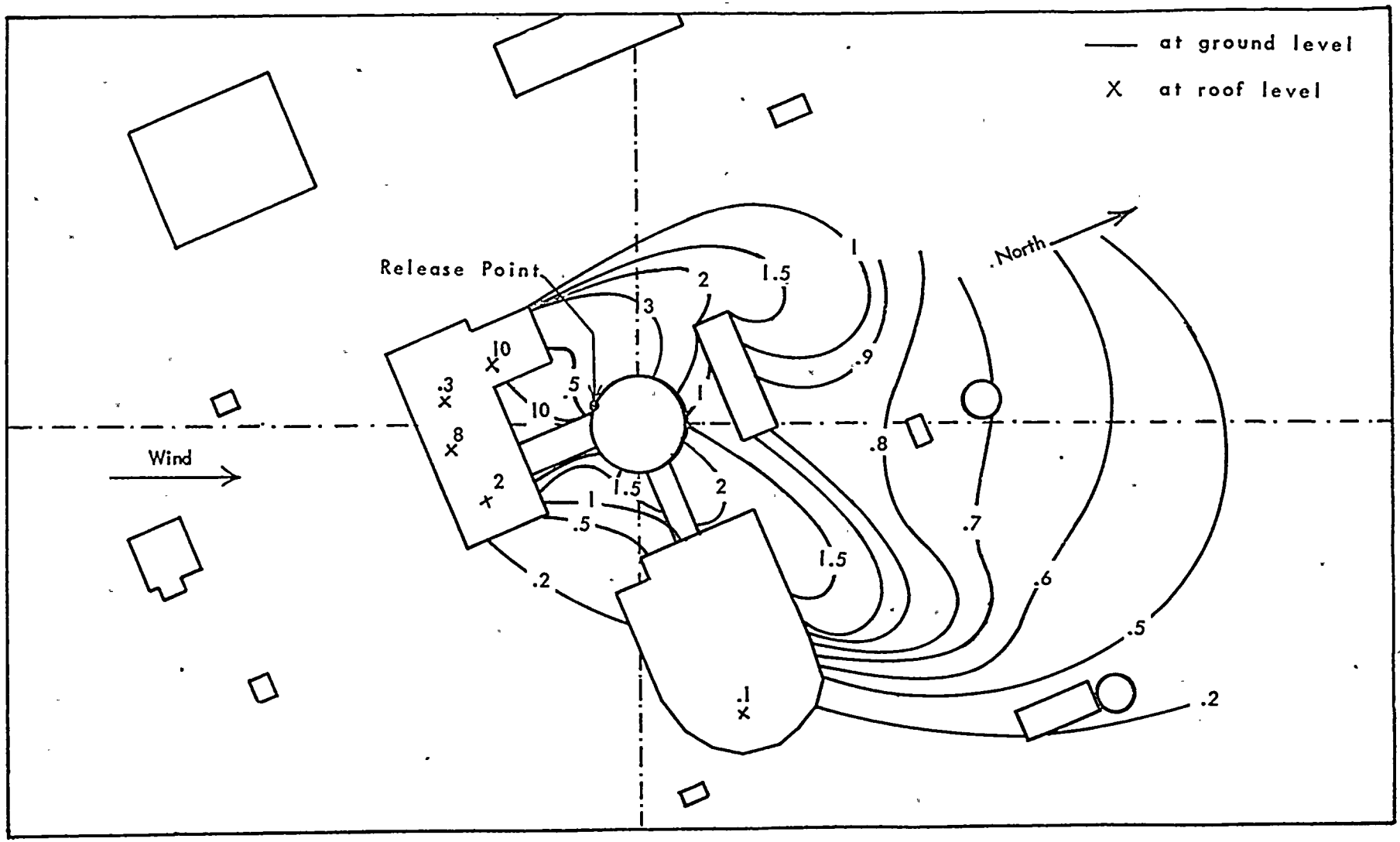

Fig. 28 K - Isopleths for Gas Released through Reactor Shell

Configuration	:	entire complex
Release point	:	bottom upwind
Wind	:	SSW, log profile, 5.54 fps

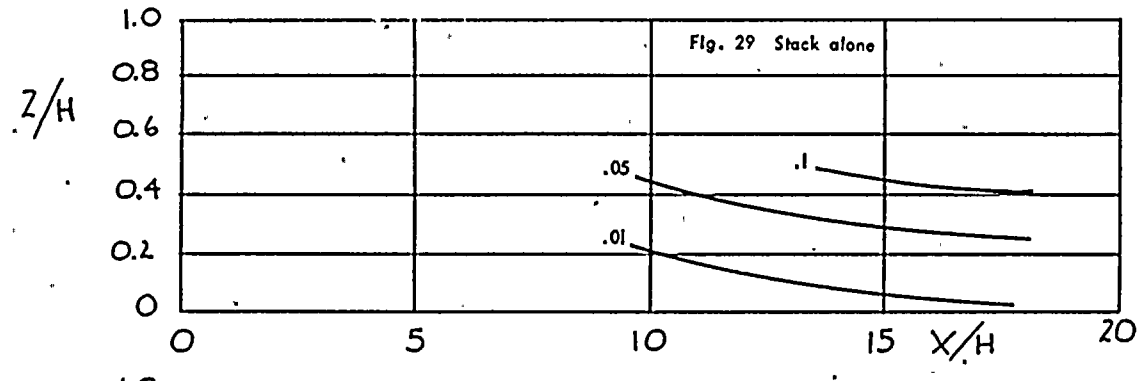

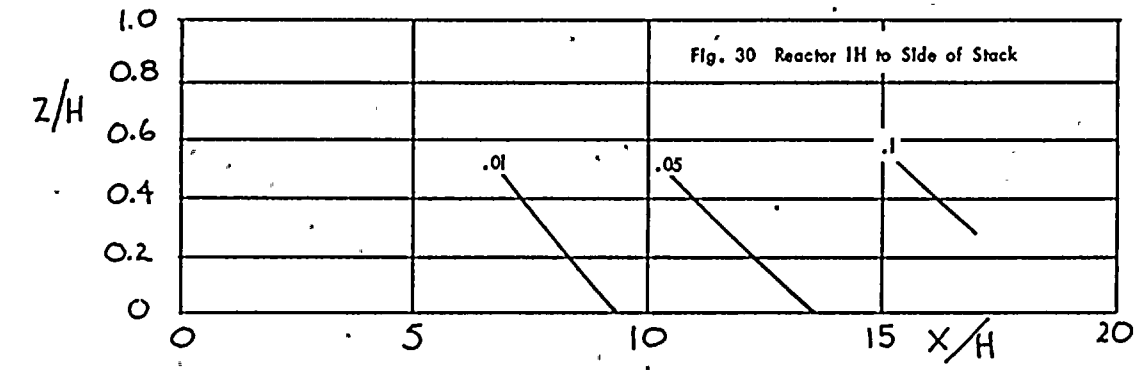

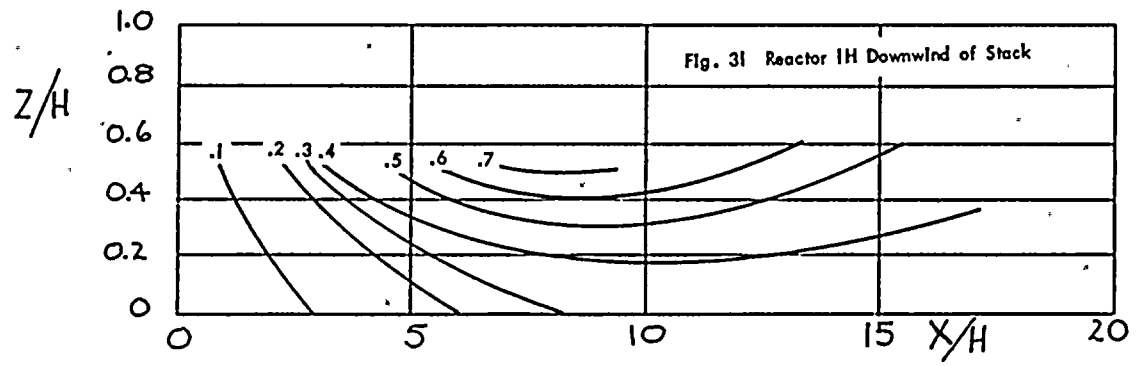

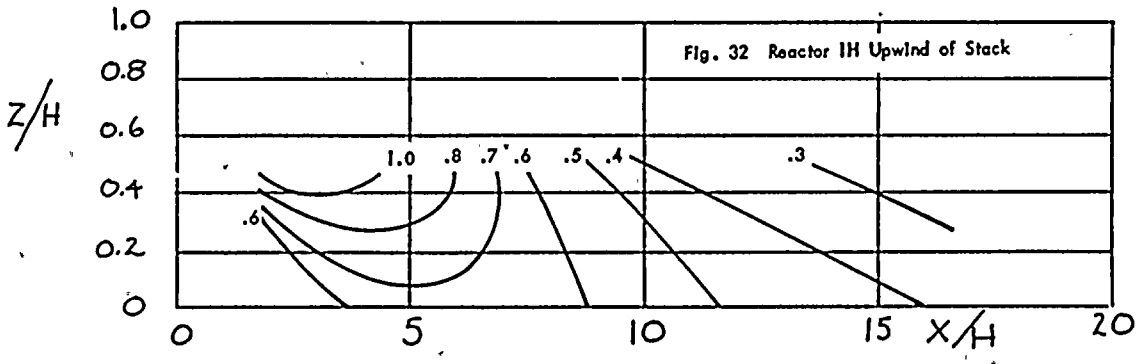

Figs. 29 to 32 K - Isopleths for Gas Released through 98 ft. Stack

Configuration	:	stack with and without reactor shell
Release point	:	top of stack
Wind	:	log profile, 5.54 fps
Origin of coord.	:	base of stack

H = Reactor height = 98 ft.

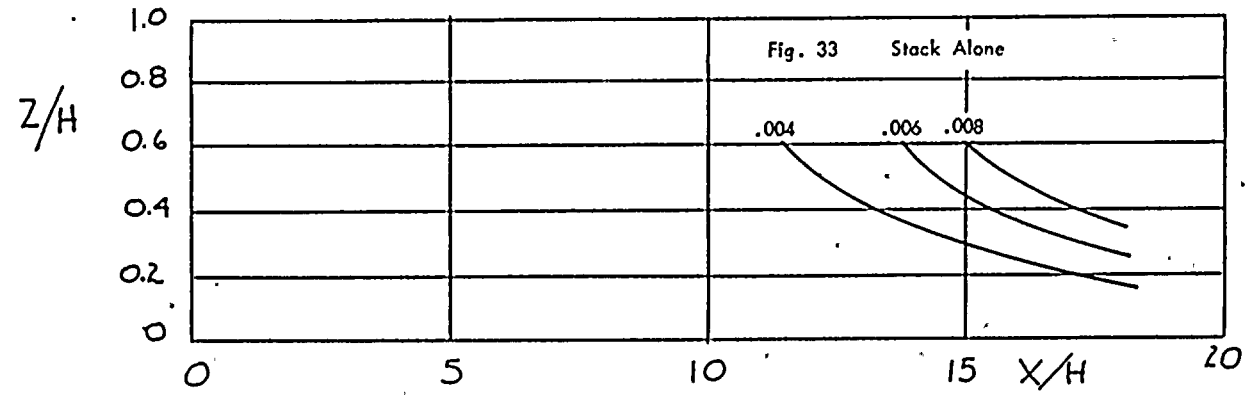

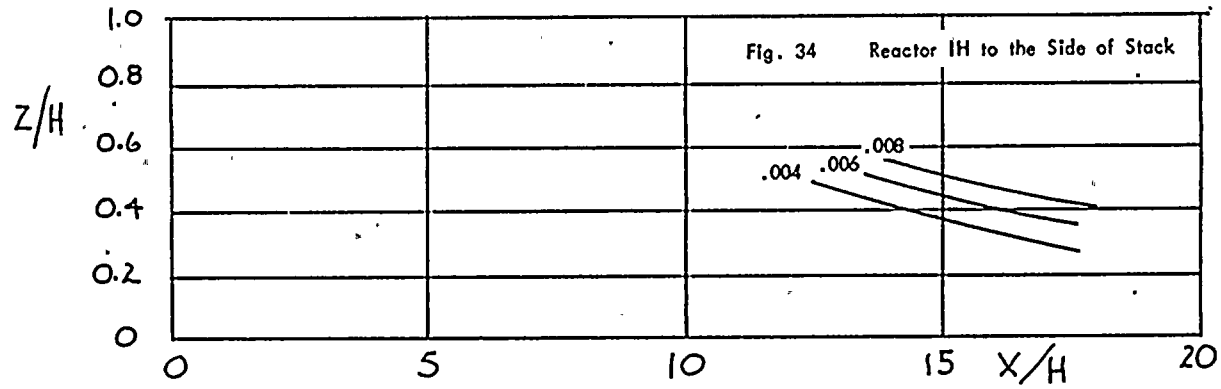

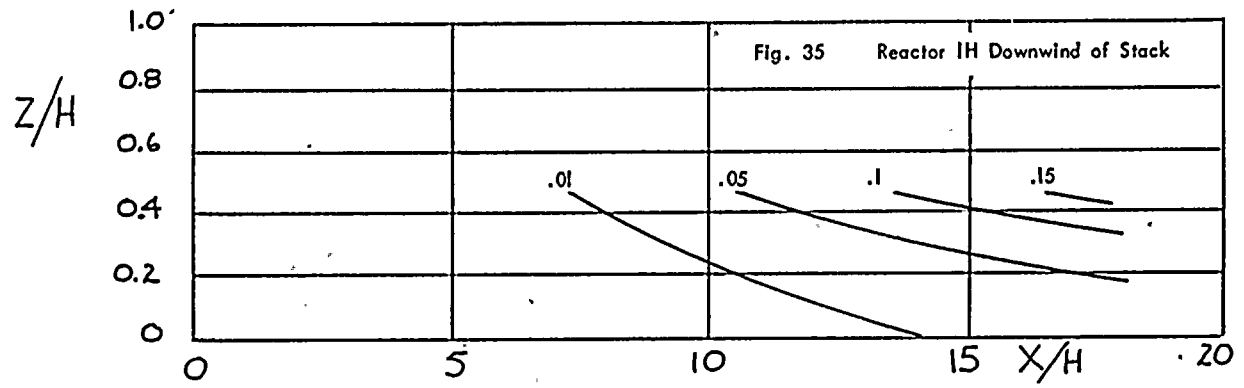

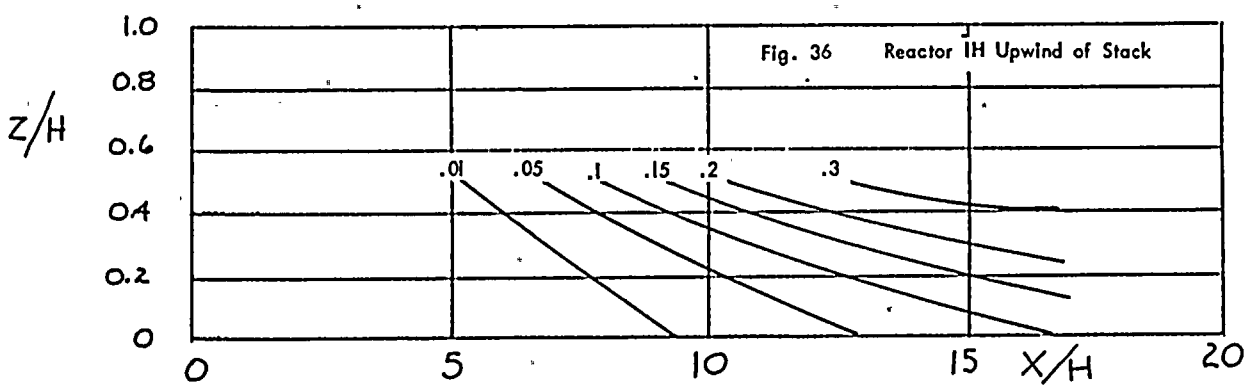

Figs. 33 to 36 K – Isopleths for Gas Released through 147 ft. Stack

Configuration : stack with and without reactor shell
Release point : top of stack
Wind : log profile 5.54 fps
Origin of coord.: base of stack
H = Reactor height = 98 ft.

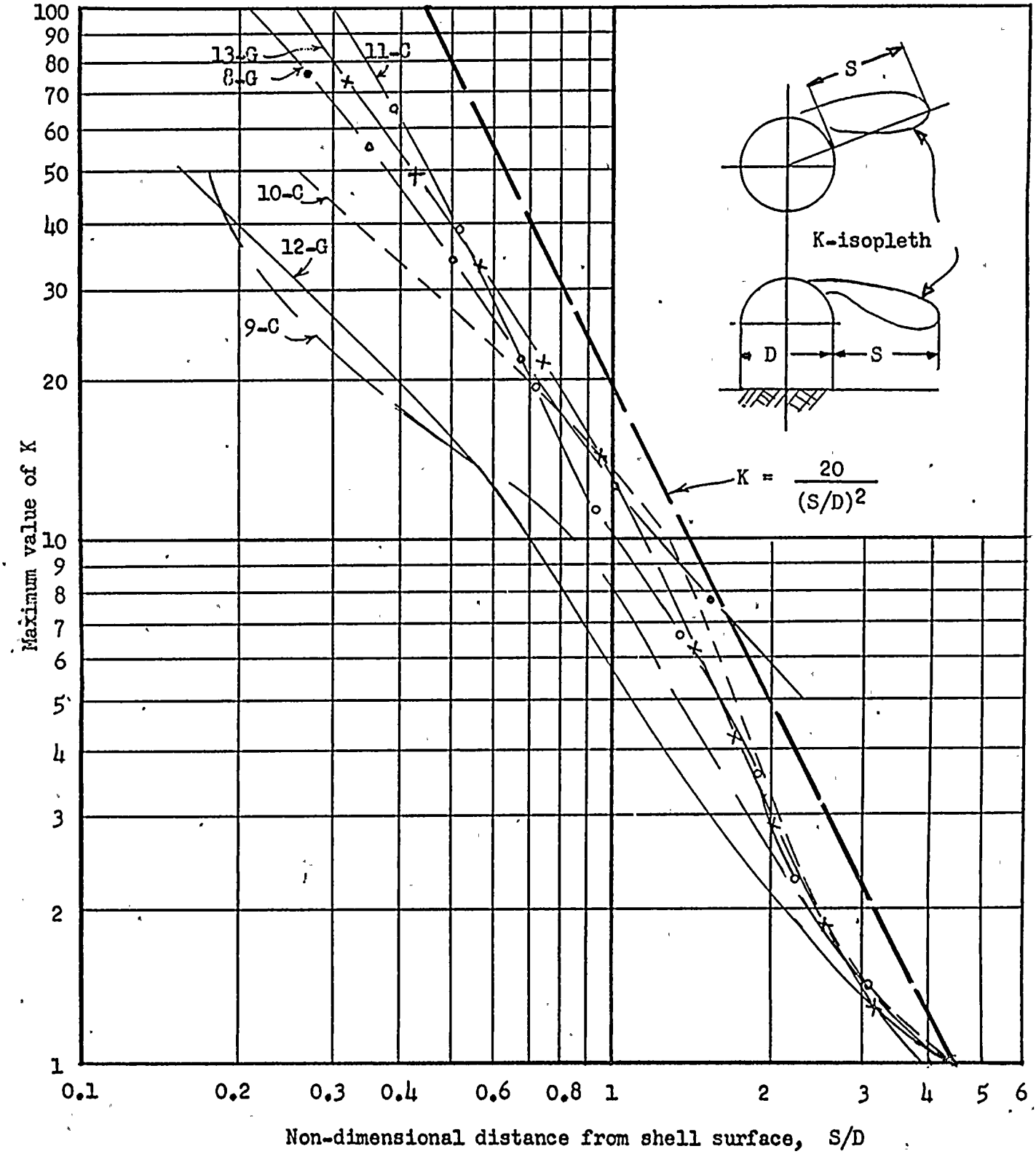

Fig. 37 Maximum Value of K vs Distance from the Shell

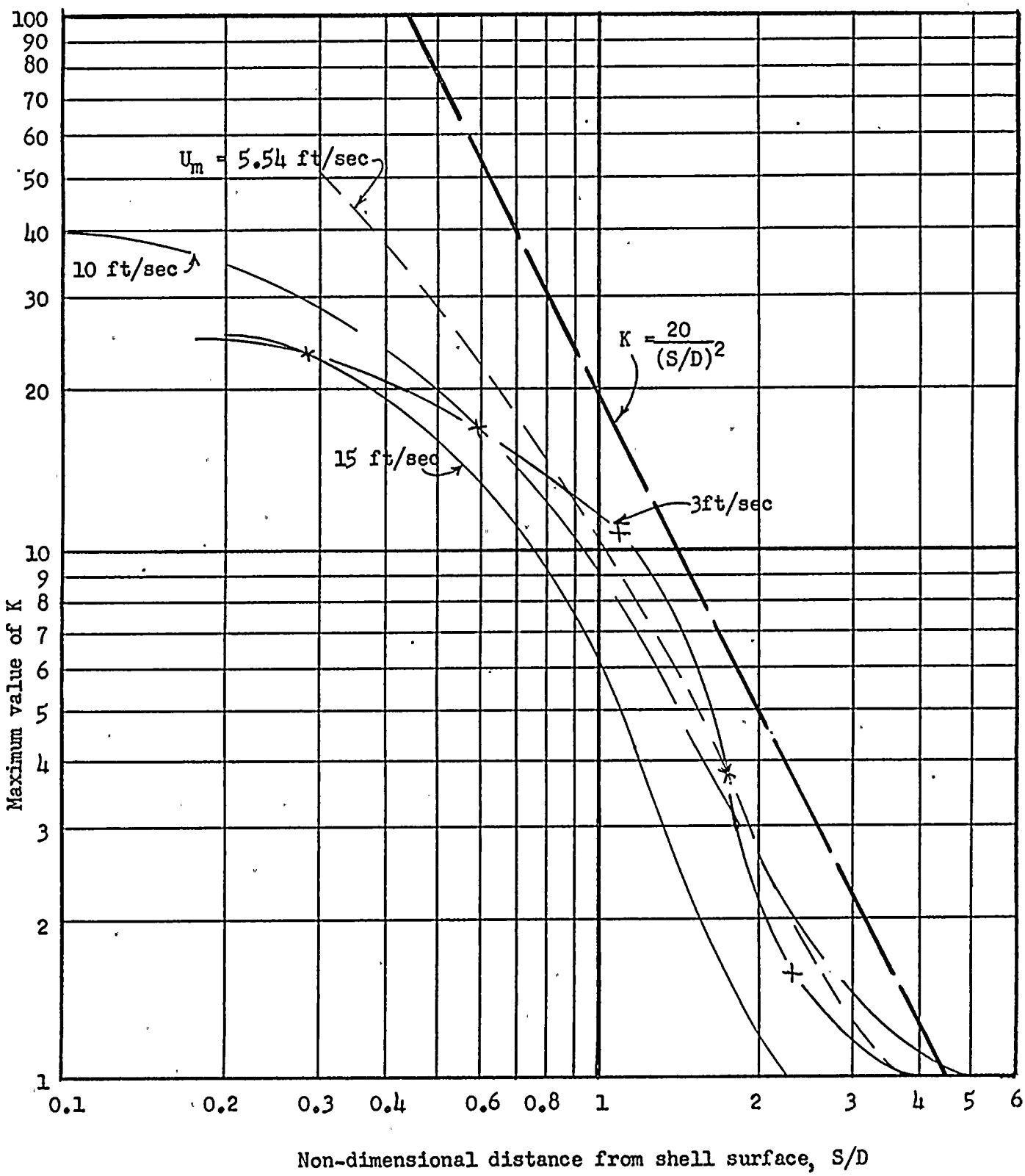

Fig. 38 Dependence of Maximum Value of K on Wind Velocity